Design, Fabrication and Characterization of Bio-Inspired Micro-Nano New Generation Polymer Fiber Array

Biolojiden Esinlenmiş Yeni Nesil Mikro-Nano Polimer Fiber Dizini Tasarımı, Üretimi ve Karakterizasyonu

PEYMAN ANSARI

Hacettepe University

This is prepared as master thesis which is predicted by director of education and examination of master education for Mechanical engineering department.

2013

To institute of graduate studies in science,

This work is accepted as **MASTER THESİS IN MECHANICAL ENGINEERING DEPARTMENT** by our jury.

President :…..
Asst.Prof. İlker Murat Koç

Supervisor :…..
Dr. Bilsay Sümer

Member :…..
Asst.Prof. Benat Koçkar

Approval

This thesis is deemed appropriate in accordance with the relevant provisions of director of education and examination of master education of Hacettepe University in ...../...../........ by above jury members and is accepted by director committee of institute in ...../...../........ .

Prof. Dr. Fatma Sevin Düz
Director of Institute of Graduate Studies in Science

BİOLOJİDEN ESİNLENMİŞ YENİ NESİL EYLEYİCİ ve ALGILAYICI TASARIMI VE ÜRETİMİ

Peyman Ansari

Öz

Tezin ana amacı biyolojiden esinlenilmiş sentetik polimer fiber dizisi tasarlamak, üretmek ve karakterize etmektir.

İki yüzeyin birbirine güçlüce yapışması ve kolayca aynı yüzeyden herhangi bir iz bırakmadan ayrılması birçok teknolojik alanda istenen bir olgu olsada nadir olarak insan yapımı yapılarda başarılabilir. Bu yapışma ve ayrılma olgusunu (tersinilebilir yapışma), doğa, binlerce yıllık deviniminde çeşitli hayvanların hareket ayaklarının üzerinde fiber dizini şeklinde gelişerek başarmıştır. Bu yapışmanın yüzeyler arasındaki moleküler çekim gücünden (van der Waals kuvvetleri) kaynaklandığı düşünülmektedir. Gecko hayvanı ayakuçlarında bulunan fiber yapısı vasıtasıyla burada sıralanan özelliklere sahiptir ve bunlar aynı zamanda bu tezde sentetik olarak üretdiğimiz fiber dizininde ulaşmaya çalışacağımız özelliklerdir:

- Düz ve değişik yüzey pürüzlülüğü sahip yüzeylere tutunabilme,
- Ağırlığının yüzlerce katı kadar tutunma gücüne (adezyon kuvvetine) sahip olma,
- Tekrar edilebilir yapışkanlık özelliği,
- Kendi kendine temizleme özelliği.

Bu kapsamda öncelikle yumuşak zemin üzerinde bulunan (destek katmanı) mikro-nano fiber dizisi için sürekli temas mekaniği modelleri ve sonlu elemanlar metodu kullanılarak bir yüzey ile olan yapışma durumları, modellenmiştir. Sonlu elemanlar metodunu kullanarak fiberler tasarlanmıştır. SEM'de fiberler statik halde değişik güçlere maruz kalarak onların gösterdiği yer değişim ve mukavemet araştırılmıştır. Yumuşak litografi yöntemiyle fiberler mikro-nano boyutunda değişik çaplarda ve boylarda üretilmiştir. Fiberler üzerinde deneyler yapılarak, fiberlerin farklı pürüzlüklerde yüzeylerle adaptasiyonu araştırılmıştır.

Anahtar Kelimeler: Biyolojiden esinlenmiş fiber, Tasarım, Üretim, Pürüzlük, Çekme

Danışman: Dr. Bilsay SÜMER, Hacettepe Üniversitesi, Makina Mühendisliği Bölümü

DESİGN AND FABRICATION OF BIO-INSPIRED NEW GENERATION TACTILE SENSOR AND ACTUATOR

Peyman Ansari

ABSTRACT

Design, fabrication and characterization of micro-nano bioinspired fiber array is the main idea of this thesis.

Even though adhesion of the two surfaces together powerfully and easily separation from the same surface without leaving any trace is a desired phenomenon in most technological area, but it is seldom achieved in man-made structures. Nature has done this adhesion and separation phenomena (reversible adhesion) in various animals by fiber arrays on their motion foot during thousands of years. It is considered that this adhesion arises from molecular attraction force between surfaces (van der Waals forces). Gecko owes features listed here by toes (fiber structure found on foot ends of gecko), therewithal these are features which is tried to achieve in fabricated synthetic fiber arrays:

- Holding on smooth surfaces and surfaces with various roughness values,
- Have the power to carry weight up to hundreds times of its weight (adhesion force),
- The repeatable adhesion feature,
- The self-cleaning feature.

In this context primarily, using continuum contact mechanics models and finite elements method, adhesion situations of the micro-nano fibers on backing layer is modeled. Fibers are designed using finite elements method. In FEM different forces are applied on fibers and resultant displacement and stress is examined. Fibers in various diameter and height are fabricated by soft lithography method. Then experiments are done to find the adaptation of fibers with different rough surfaces.

FORWARD

Bu çalışmanı hər zaman dağ kimin arxamda olan ailəm başda olaraq, Azərbaycan xalqına sunuram. Dr.Bilsay Sümer cənablarına verdiyi əmək və çalışma boyunca çəktiyi zəhmətlər için təşəkkür edirəm. Hər zaman dəstəyini əsirgəməyən sayqı dəyər yoldaşım Morteza Yeganehpour cənablarına təşəkkür edirəm.

Ümid edirəm azad Azərbaycanımızda bilim sahəsi başda olaraq, bütün sahələrdə dünyada öncül və örnək xalq və ölkə olaq.

<p align="right">**Peyman Ansari**</p>

Ethics

In accordance with the thesis writing rules of institute of graduate studies in science of Hacettepe university, during preparing of this thesis I declare that,

- All data and documents in thesis are obtained in accordance with the academic rules,
- All audio-visual and written data and results are presented in accordance with scientific ethic rules,
- In accordance with scientific norms if the works of some other ones is used, citations are given,
- All works that has been cited, are shown as references,
- No falsify is done one used data,
- And any part of this thesis is not presented as another thesis work in this university or some other university.

28/06/2013

Peyman Ansari

TABLE OF CONTENTS

LIST OF TABLES

LIST OF FIGURES

1. Introduction

Adaptation properties of Gecko foot in contact with surfaces are the role model to develop pressure sensitive adhesives. Their rapid, powerful and repeatable attachment and detachment talents are striking. These magnificent talents of gecko are based on the millions of micro/nano-scale setae structures on its toes. The size, shape and the density of the micro/nano structures are the most important factors affecting the adhesive strength of them. The repeatable adhesive strength of these micro/nano structures on even smooth or rough surfaces is the desired property for an artificially made fibrillar structures.

1.1 Micro Fiber Manufacturing Techniques

Respecting the role of micro fabrication in microelectronics and optoelectronics, it is an indispensable contributor to information technology [1]. Micro fabrication is ever-present in various branches of technology such as fabrication of combinatorial arrays [1], micro reactors, sensors [2], micro electro mechanical systems (MEMS) [3], micro optical systems [4] and micro analytical systems [5]. Micro fabrication uses several kinds of patterning techniques that the most effective kind is photolithography [6]. In MEMS almost all fabrications are done by this method [4]. Another method which is named project photolithography, projects absolute pattern onto photoresist simultaneously [7]. By photolithographic techniques we are able to mass producing of the structures in sizes as small as 250 nm [8], and it is believable to catch 100 nm size in near future using combination of deep UV light (e.g. 193 nm argon fluoride (ArF) excimer laser or 157 nm F_2 excimer laser) and improved photoresists [8]. The optical methods cannot overcome mentioned 100 nm barrier, which is a critical point in the reduction of feature sizes set by combination of short-wavelength cutoff and optical diffraction to the transparency of the optical materials used as lenses. Instead progressive lithography techniques are being explored for conventional photolithography in the regime <100 include extreme UV (EUV) lithography, soft X-ray lithography, e-beam writing, focused ion beam (FIB) writing, and proximal-probe lithography [9]. Mentioned techniques have proficient to fabricate extremely small features (in nano meter ranges). To develop them to reach

mass-production level and fabricate in wholesale range more effort is required still. EUV and X-ray techniques, for example, require the development of reflective optics and/or new types of masks, and arrays of beams or some form of flood illumination rather than a single beam must be developed in e-beam or FIB writing; all require new ideas for mask maintenance and repair and for dealing with problems such as nonplanarity in the substrate [1]. Despite the fact that the dominant technology is photolithography, even for large (µm- scale) features, it is not the only or the best method for all implementations always. Photolithography is not a cheap technology [7, 10, 11]. It is not suitable for patterning non planar surfaces, because it has not any control on the chemistry of the surface and that's why it is not suitable to generate patterns of specific chemical functionalities on surfaces. By photolithography only two-dimensional microstructures can be generated and it can be applied on only limited photoresists [12]. Photolithography is more used micro fabrications based on photoresists more that other materials because of its characteristics. Attaching chromophores or add photosensitizers it is possible to work with other materials.

1.2 Roughness Adaptation of Micro Fibers

Surfaces which we assume them smooth, are not smooth in real. All surfaces have roughness on many different length scales. As we get two bodies in contact with each other, the contact area between them is not nominally flat surface of them. The real contact area is only a small friction of nominal surface because of the roughness of contacting surfaces. Respecting to the elastic or plastic deformation of asperities on surfaces, contact regions can imagine like small regions in which asperities from one solid are compressed against asperities of other solid. The fundamental point is the real contact area value. Knowing real contact area has huge important effects. For example it decides the heat transfer and contact resistivity between contact solids. It is also very important for sliding friction [13]. It has a major effect on the adhesive force between two solid in direct contact. For elastically soft solids adhesion has a special importance. As two solids are in direct contact it may pull both bodies over the whole nominal contact area [14]. In robots and their contact mechanics with surfaces, adhesion force plays a very big

role. The pull-off force of robot wheels is one of the major problems. The wheels get into contact with various rough surfaces. Surfaces which has various RMS values and directly affect the pull-off force of robot wheels. Accordingly the simulation of rough surfaces and simulating their contact with solids carries a huge important [15-17].

1.3 Adhesion of Micro-Fibers

One of the basic issues in MEMS building is scale effect [18]. Increasing the ratio of the surface to volume when MEMS dimension decreases, cause to challenging issues. The forces which affect micro scale devices are different with those which affect devices with conventional scale. Its reason is the size of a system that bears a meaningful effect on the physical phenomena that dictate the dynamic behavior of that system. For example smaller scale systems are affected by inertia effects very little reverse of the large scale systems. While smaller systems are influenced by surface effect more than others.

Basic problems which limits both operational lifetime and fabrication yield of many MEMS devices are powerful adhesion, friction and wear which caused by surface effect [19, 20]. Powerful adhesion usually is result of capillary, electrostatic, van der Waals forces, and other kinds of chemical forces [21, 22]. Stiction is a term that has been applied to the unintentional adhesion of compliant microstructure surfaces when restoring forces are unable to overcome interfacial forces. The stiction problem of MEMS can be divided into two categories: release-related stiction and in-use stiction. During the process of sacrificial layer removal in fabrication of microstructures, release-related stiction occurs, and primarily such stiction is caused by capillary forces. Upon exposure of successfully released microstructures to a humid environment causes in-use stiction. Figure 1.1 illustrates stiction of micro cantilevers to the substrate. Figure 1.2 shows the adhesion between the fingers of a comb structure in a micro machined accelerometer.
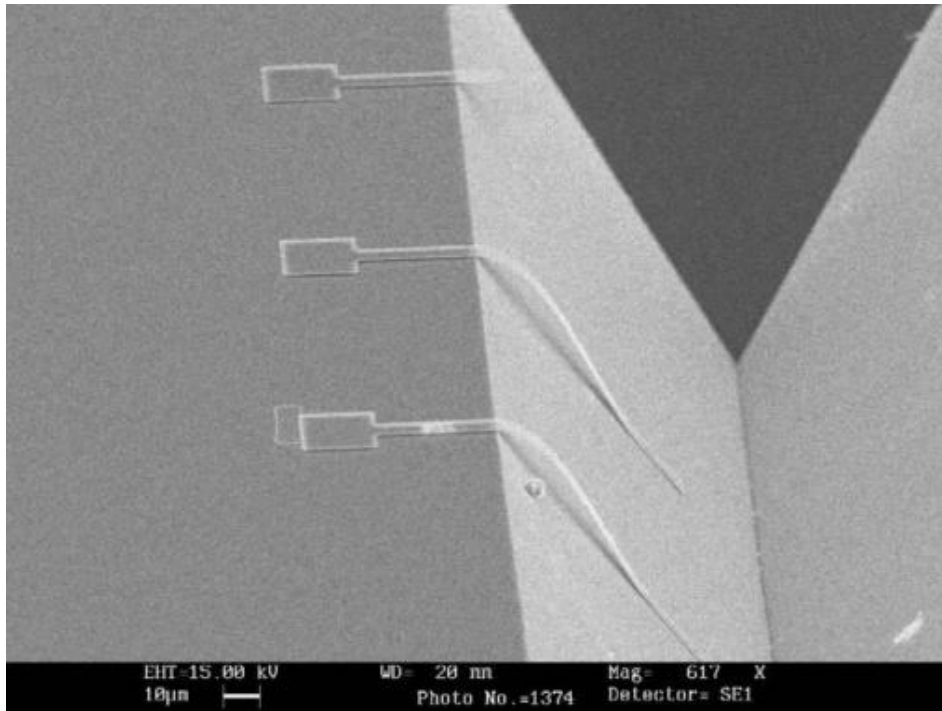
1.1 Stiction of microcantilevers to substrate [23].
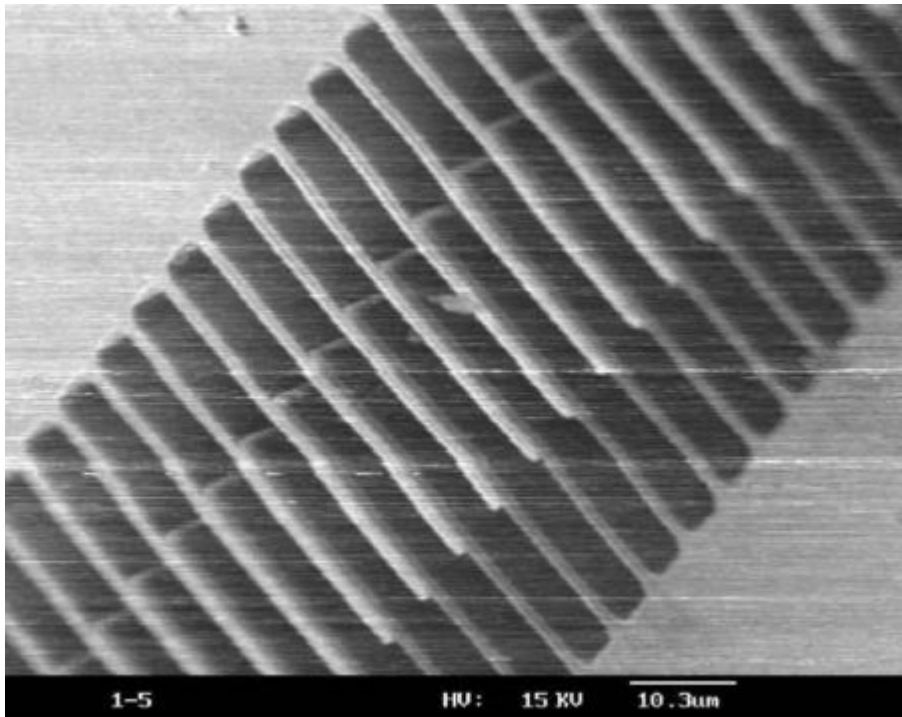
1.2 Adhesion between fingers of a comb structure in a microaccelerometer [23].

Early experiments with a soft rubber sphere in contact with glass exhibited that how much the adhesion subject is important. These experiments guided to the development of mechanical theories of adhesion of elastic spherical surfaces, which led to credibly calculation of Hertzian contact areas in the presence of adhesion. In these theories value of relative magnitude of the adhesion varies inversely with the product of the contact size and equivalent elastic modulus of the two surfaces. Experiments with rubber show that the contact size is relatively large (millimeters), but the equivalent elastic modulus is small. Experiments, which are performed with nanoprobes, show that equivalent elastic modulus is large but the contact size is small (nanometers). Surface roughness plays a very significant role on the magnitude of the pull-off force. Pull-off force is defined as: force which is needed to separate two bodies after brought into contact.

2. Design of Micro Fiber Arrays

Design of micro fiber arrays is done to prevent failure of fibbers. Buckling, matting and defect resistance failure situations are examined. Every one of these failure conditions lead to failure of fibrillar structure. Therefore the first step in manufacturing is to design and identify the critical failure values of every variable factor.

Each pillar is modeled as a linear spring in loading direction, and the following assumptions are applied (Figure 2.1):

- Each fiber is considered as a cylindrical beam going under small changes,
- Boundary conditions are considered as one end fixed and one end free beam,
- Tip of fiber is limited to move just in vertical direction,
- Shear force at the interface does not occur in any way,
- Neighbor fibers are independent of each other mechanically,
- Pillars are considered to be elastic.
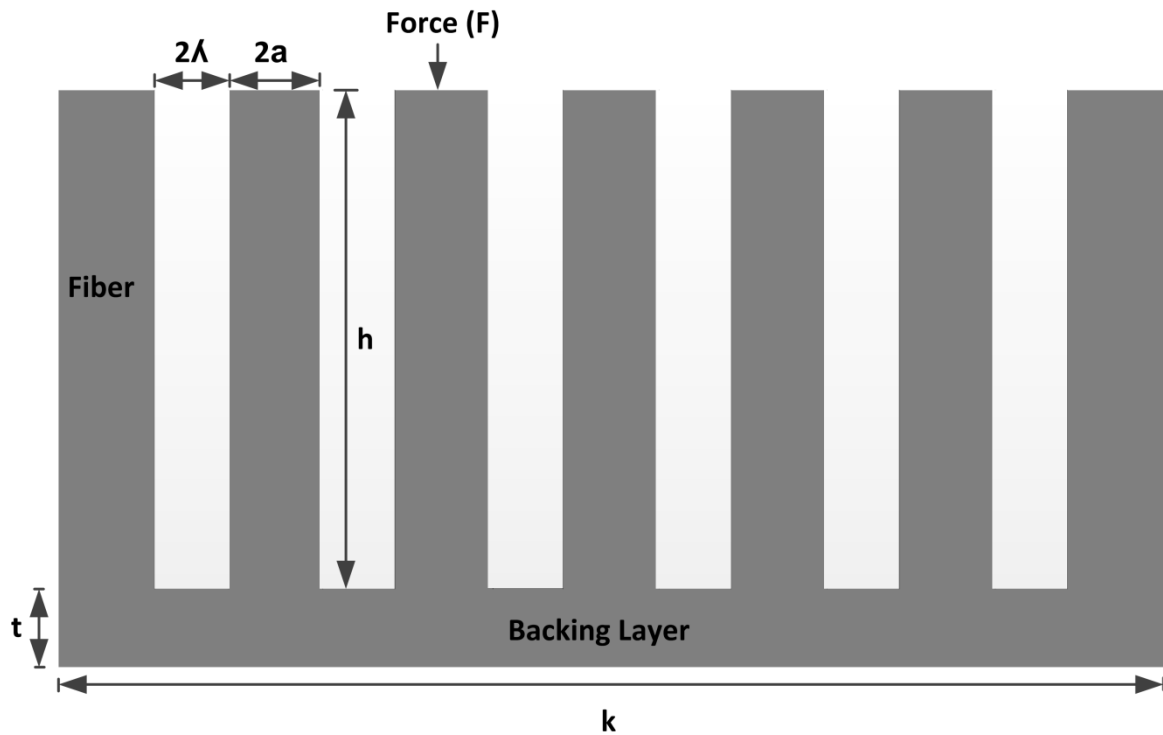
2.1 Fiber array schematic.

Mechanical modeling of vertical pillar array was performed using MATLAB program and is described in following sections.

2.1 Elastic Buckling Failure

To increase compliance of fibers to rough surfaces and increase the adhesion of fibers to surface, high aspect ratio is preferred [24]. As the aspect ratio of fiber increases, the effective elastic coefficient of fiber decreases and adhesion increases. Just if fiber squeezes under any preload, fiber could go under buckling destruction failure (instability) at the lower amounts of material's strength values after some specific displacement. Based on classical Euler buckling, for a uniform applied stress, micro-buckling occurs when the force normal to the fibril exceeds a critical value, F_{cr}, given by [25] [26],

$$F_{cr} = b_c \frac{\pi^2 E^* I}{h^2} \tag{2.1}$$

where F_{cr} is applied critical vertical load on pillars, $E^* = E/(1 - \vartheta)^2$ is the plane strain fibril modulus, ϑ is Poison's ratio, E is Young's modulus, $I = \pi(2a)^4/64$ is the area moment of inertia and b_c is a factor of the order of the unity which depends on boundary conditions. b_c is equal with 2 for pinned–clamped micro-beams [25].

Figure 2.2 versus critical stress with aspect ratio respecting Equation 2.1.
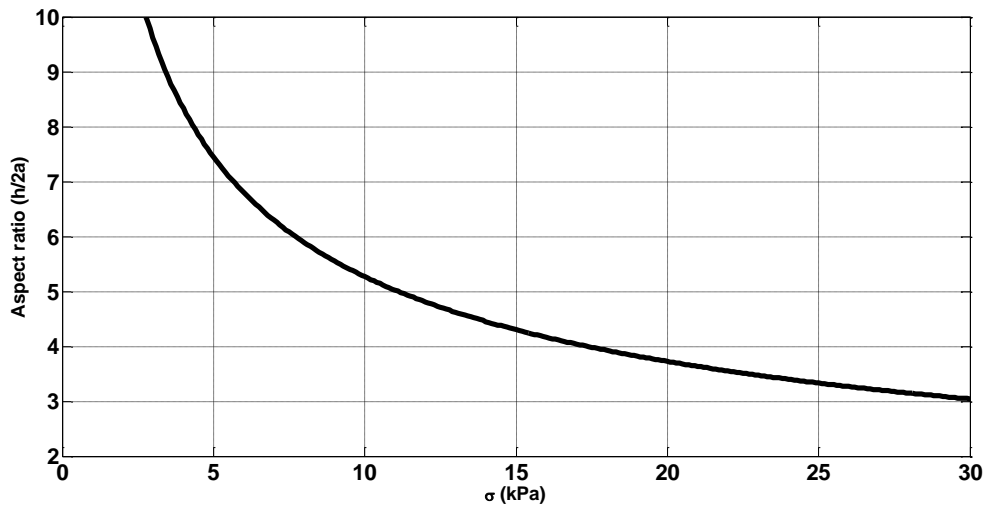
2.2 Stress versus aspect ratio (h/2a).

2.2 Matting Failure

Numbers of fibers which can be placed per unit area, in other words, lateral resolution, depend on the gap between two fibers. To place fibers intensive the gap between fibers is looked forward to be the lowest value. If fibers are fabricated in high aspect ratios, because of the adhesion force between them or by any small fluctuations resulted from surface contacting, fibers may stick each other. This sticking situation is fiber collapsing and specifies physical limit to fiber density. The lateral collapse occurs when gap between fibers is not sufficient [26],

$$\left(\frac{\pi^4 E^* a}{2^{11}\gamma_s}\right)^{1/12} \left(\frac{12\, E\, a^3 \lambda^2}{\gamma_s}\right)^{1/4} > h \tag{2.2}$$

where γ_s is the surface energy.

2.3 Defect Resistance Failure

In solid mechanics contact of a circular flat end fiber with a flat surface is the problem of contact of a circular flat punch with a flat surface and interaction equation is given as [26],

$$F_a = \sqrt{\frac{3}{4}\pi(2a)^3 E^{**}\omega_{ef}} \tag{2.3}$$

where F_a is the force of adhesion, ω_{ef} is the effective work of adhesion, $E^{**} = 4/3\,[(1-\vartheta_1^2)/E_1 + (1-\vartheta_2^2)/E_2]^{-1}$ is the effective elastic modulus, E_1 and E_2 respectively are surface and fiber elastic modulus, ϑ_1 and ϑ_2 respectively are surface and fiber Poison ratio.

If adhesion force of a fiber is controlled by its interface adhesion properties more than spread slit, this fibers adhesion situation can be called insensitive to error. Pulling off from the surface (as fiber is under stress), fibers which are unresisting to defects, prior the cracks begin to form in the lining of fiber and then cracks start to progress toward the center of the fiber, separate from surface. As a result of this situation work of adhesion results lower than expected. In fibers which are resisting to defects average work of adhesion is almost equal to the interfacial adhesion pressure $(\sigma_{interface} = 4F_a/(\pi(2a)^2/4))$ and is more near to the theoretical adhesion value expected for the fibers. This is an important design criterion, because it cannot be guaranteed that the face of the surface which fiber contacts (or will contact) with is flat and smooth. The defects which are defined here are conformational disorders on fibers which occur during fabrication of fibers. For the example; the tip surface of the fibers which are fabricated cylindrical never cannot be pure flat, but generally in calculations dimensional surface of the fiber is assumed to be stable and smooth. So the fibers that will be fabricated

should be defined resistant to the defects, in other words, they should give the theoretical adhesion force not affecting from the defects which may occur during the fabrication process.

2.4 Mechanical Design

The critical values for elastic buckling, matting and defect resistance failures are calculated and drawn by MATLAB program.

In MATLAB simulations fiber's diameter and gap between them is changed in 0-150 μm interval and the corresponding critical height respecting above mentioned equations is determined. Using data obtained from these simulations, critical lateral adhesion and buckling destruction graphs are drawn (Figure 2.3(a) and Figure 2.3(b)). According to this, for any gap and diameter critical height should be under this graph. For critical lateral adhesion destruction as, diameter and gap between fibers increases, critical fiber height increases too. In buckling graph for low gap values, as diameter of fiber increases critical height of the fiber increases too. For a constant diameter, by increasing gap between fibers, critical height decreases. Defect perfection ratio does not depend on gap between fibers and for any height, diameter should be less than 103μm (Figure 2.3(c)). Adhesion and buckling graphs are drawn together in Figure 2.4. According to this graph in a wide range of gap variation, buckling graph's critical length value is dominant in response to any diameter change. If gap between fibers is in 0-15μm interval then for any fiber diameter value there is no proper height to coincide the lateral adhesive graph.
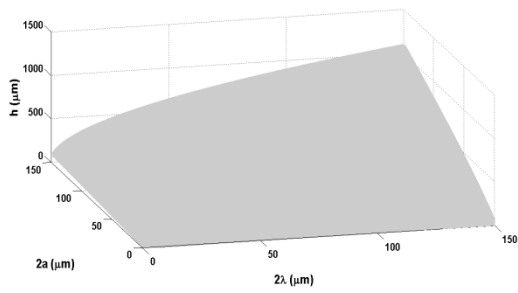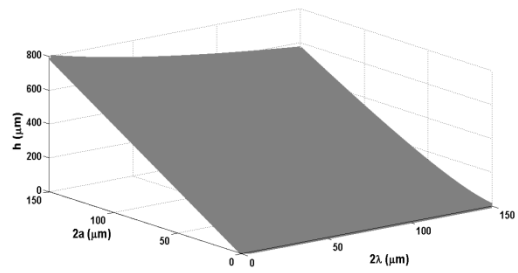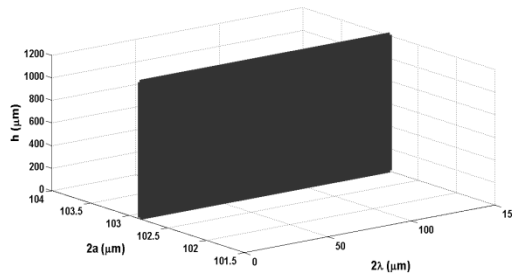
2.3 a) Critical lateral adhesion failure graph, b) Critical elastic buckling failure graph, c) Critical defect perfection graph.
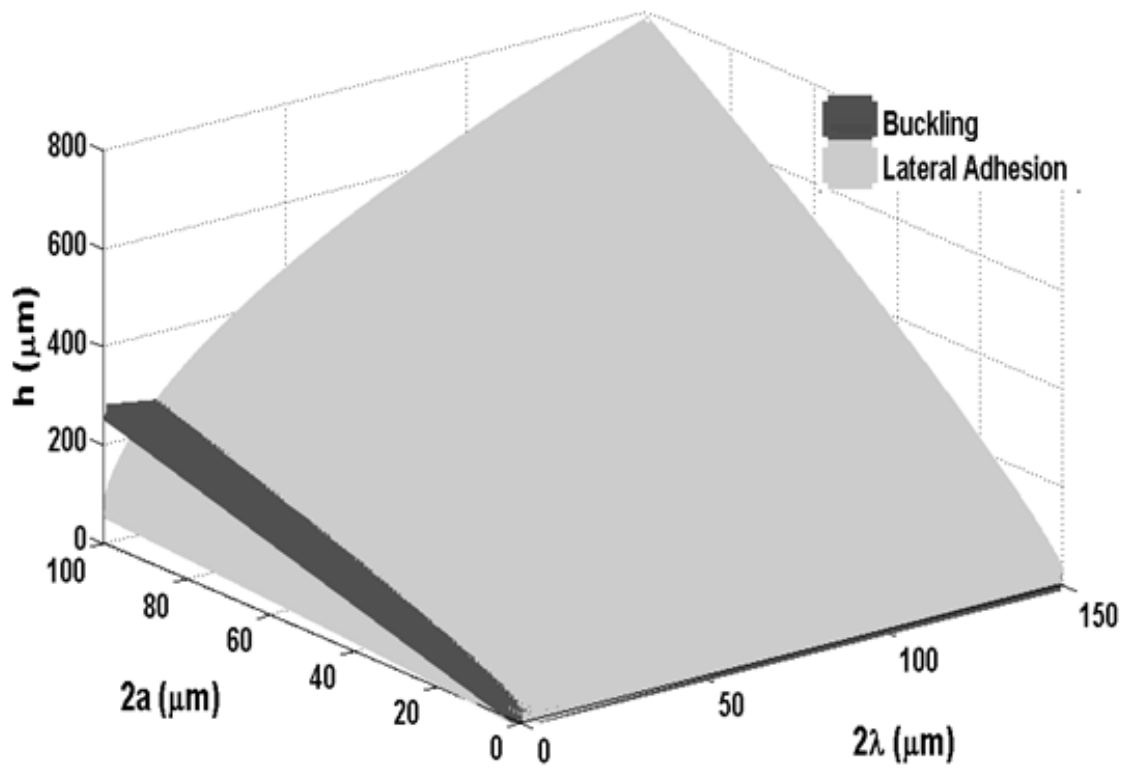
2.4 Common drawing of critical lateral adhesion destruction failure and elastic buckling failure graphs.

3. Fabrication of Fibers Using Micro Manufacturing

3.1 Micro Fabrication

In MEMS reflecting of a pattern to a photosensitive material by exposure of radiation is called lithography. Materials which their physical properties change by exposing to a radiation source are called photosensitive materials. If a photosensitive material is exposed to a radiation source by a mask, the pattern of mask will reflect on the material. We can remove the excess parts depending on material properties of photosensitive.

In MEMS lithography, photosensitive material which is used is a photoresist. As the material is exposed, its resistance to the developer solution changes. After the material is exposed it is placed in the developer and the exposed parts is etched away and unexposed parts will remain unchanged, which it occurs in positive photoresist material. If photoresist is negative unexposed parts will etch away.

3.2 Mask Design

To sheaf the pattern on the photoresist layer the glass- chrome mask is designed. The distance between fibers and their diameters are designed separately. Respecting it the 4 inch silicon wafer with 16 different fiber size is designed. Fibers have various distances between each other and various diameters as shown in Figure 3.1. L- edit drawing program is used to design the mask and it is manufactured by   DEL- 66 (Heidelberg Inst.) mask printer.

Mask Part	Diameter (2a, μm)	Distance Between Fibers (2λ, μm)	Aspect Ratio (2a/h)
1	5	5	6
2	5	8	6
3	5	10	6
4	5	12	6
5	10	10	3
6	10	14	3
7	10	18	3
8	10	25	3
9	20	16	1.5
10	20	24	1.5
11	20	32	1.5
12	20	40	1.5
13	40	20	0.75
14	40	30	0.75
15	50	80	0.6
16	60	80	0.5

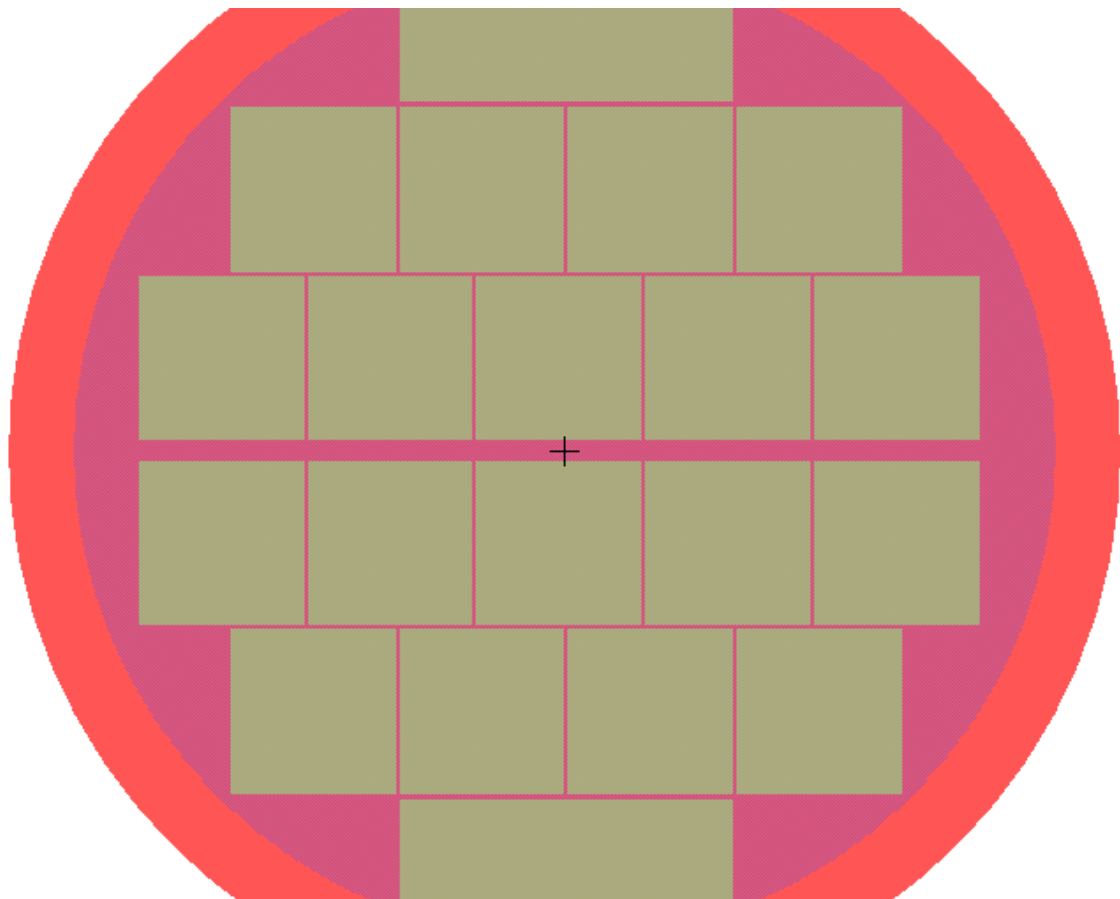**3.1** Physical properties of polymer fiber array.

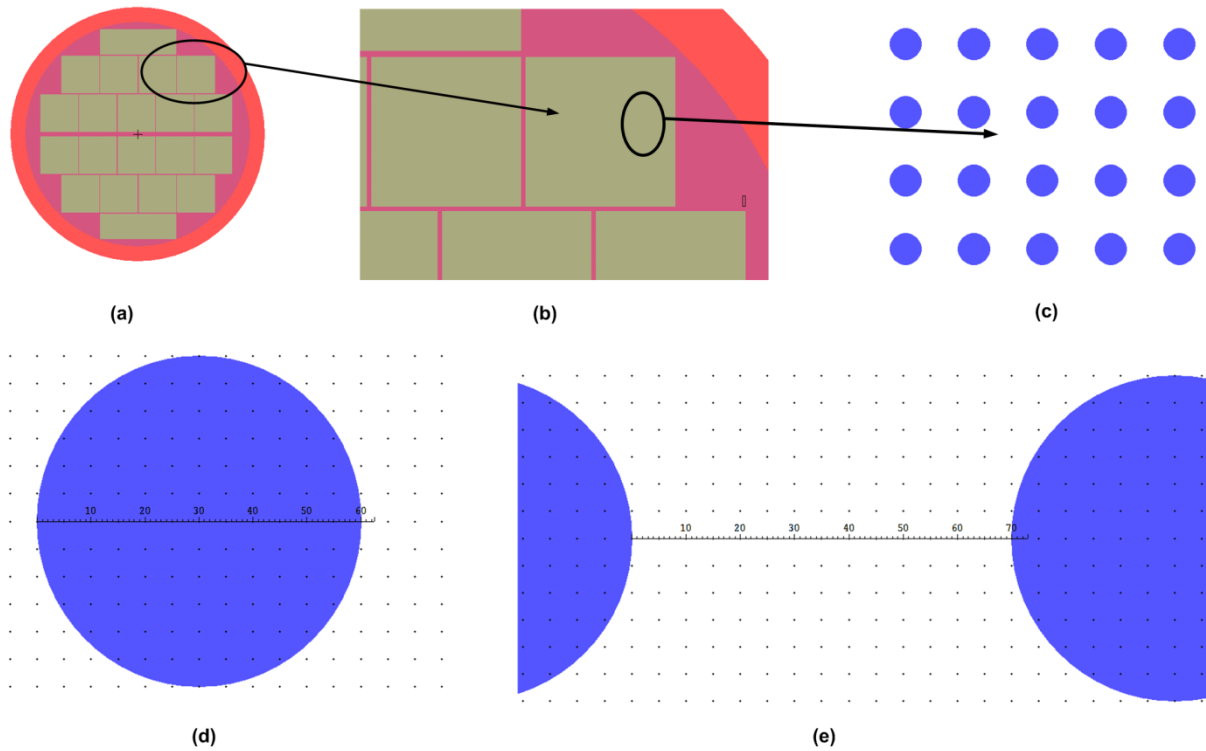**Figure 3.1** Design of mask by L-edit program. Size of the squares on mask is described in Table 3.1.

Figure 3.2 Details of the designed mask by L- edit program, a) 4 inch mask, b) Near view of a part of mask, c) Fiber array, d) Diameter of each fiber, e) Distance between fibers.
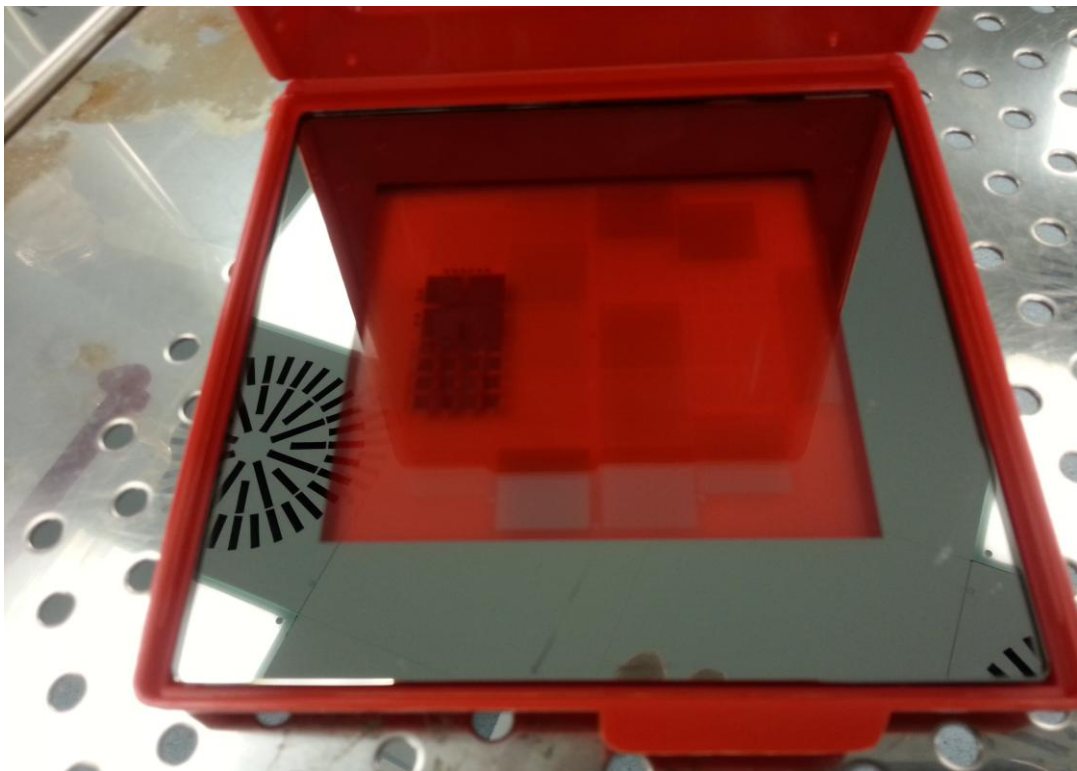

Figure 3.3 Fabricated mask which is prepared by mask printer.

3.3 Workflow of Lithography Manufacturing

3.3.1 Manufacturing

Lithography manufacturing process schematic is shown in Figure 3.4. Manufacturing method in this section starts by selecting and cleaning the wafer which process will be done on that. In this work, the size of the wafer which photolithography process will be done on is selected 4 inch. That is why the maximum diameter usable in production facilities is 4 inch.

After cleaning the Silicon wafer by Piranha wet cautery (H_2SO_4 and H_2O_2) and de-ionized water, applying vaporation method, the wafer surface is coated with Hexamethyldisilazane (HDMS) to increase the adhesion of the surface (Figure 3.4(a)). Then, negative photoresist polymer SU-8 2025 is coated on the previous surface to compose the backing layer (Figure 3.4(b)). Spin coating device is used for this process and the recipe that is followed is,

- 4 ml cyclopentanone (1:0.5) with diluted SU8-2025 (Microchem) polymer is placed on the Si wafer,

- With 100 round/min/second acceleration, device is turned for 8 second with 500/round/min velocity,

- With 300 round/min/second acceleration, device is turned for 30 second with 3000/round/min velocity,

Respecting above mentioned recipe, obtained film thickness is measured 5 μm. Then wafer is pre-baked at 95°C for 2 minutes and the resultant surface is exposed to UV lights (350-400nm) using no mask (Figure 3.4(b)). As photoresist is negative there will be no changes in physical properties of exposed photoresist. It will increase the photoresist resistance (the fibers will stand on this layer) contrasting the developer which will be applied in next level.

In next level SU8-2025 polymer is coated in 1000 round/min velocity using spin coating device and the resultant film thickness is 80 μm. Then wafer is baked at 65°C for 3 minutes and at 95°C for 7 minutes and then is returned to room

temperature. Now, using the mask which described in previous topics, surface is exposed to UV lights with 200 mJ/cm^2 energy (Figure 3.4(d)).

As photoresist is negative, no change in chemical structure will happen in UV exposed areas. Only areas which are not exposed to UV lights will experience changes in chemical structure. Then wafer is baked at 65°C for 2 minutes and at 95°C for 6 minutes. Now the pattern of the mask should appear on the wafer surface. If the pattern is not appeared on the surface, then the UV lights energy or the baking temperature was not enough probably. Next, wafer is bathed in solution with content of Acetate (1-Methoxy-2-propanol acetate). During bathing areas which has not been exposed to UV lights is solved and the structure which is negative of the mask is remained. Then wafer is washed with isopropyl alcohol and is dried with nitrogen. The resultant structure after these steps is fiber array with high aspect ratio (Figure 3.4(e)). Obtained structure is called primary mold.

Fiber fabrication is a time consuming and cost required process and in the other hand as the fibers must be obtained from flexible material, using primary mold an integrated mold is obtained. Thus Si rubber (HS II Base and Silastic 81 NW) solution is poured onto primary mold and cured. Si rubber is peeled off then (Figure 3.4(f)). Obtained structure is flexible negative mold and its fabrication is easier than the primary mold (Figure 3.4(g) and Figure 3.4(h)). So following primary main mold manufacturing workflow just one time, we can fabricate flexible mold in series and cheaply. Pouring proper polymer onto flexible mold and cure the polymer, finally by peeling polymer, fiber array is obtained (Figure 3.4(i)).
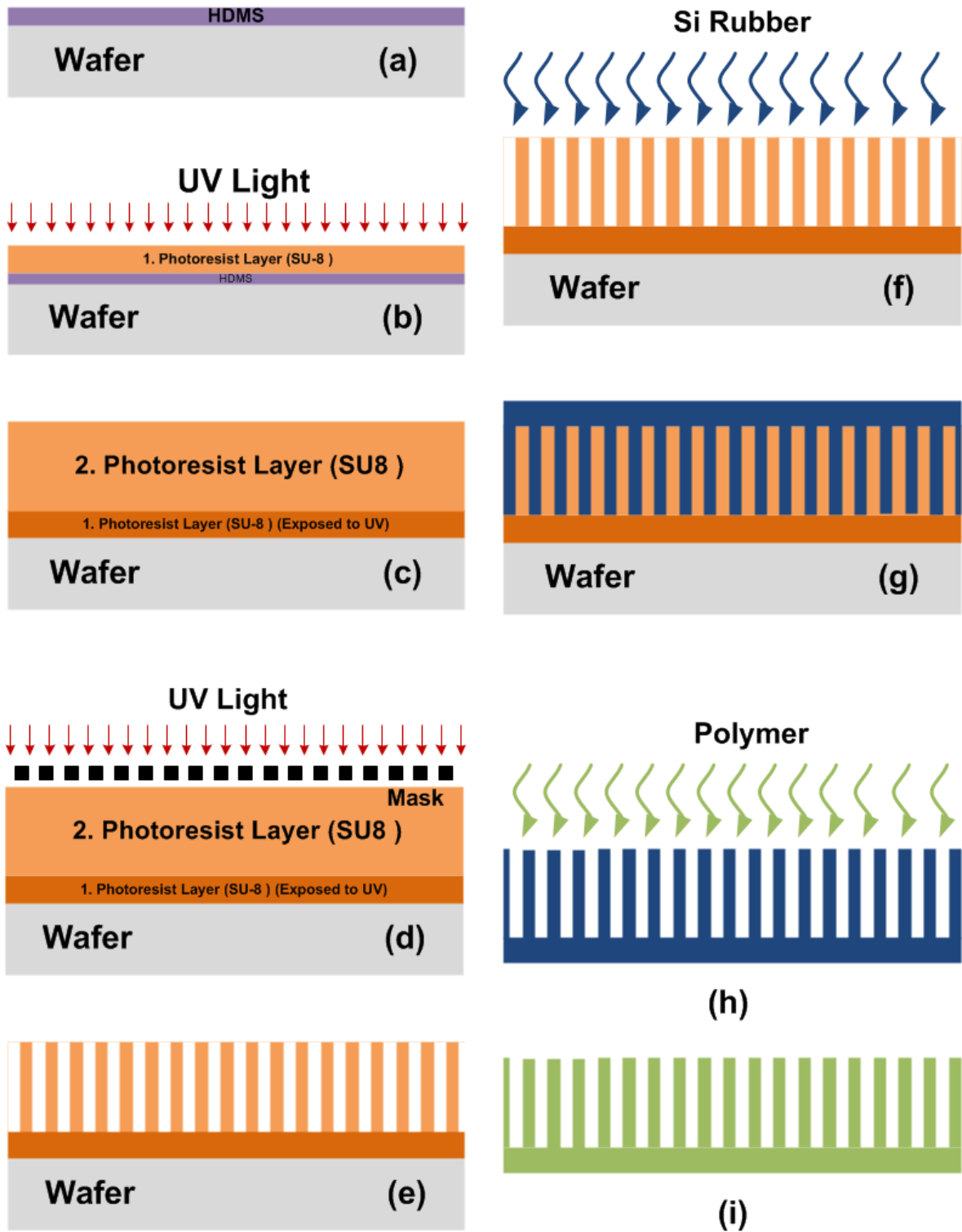
3.4 Micro manufacturing workflow schematic (SU-8).

3.3.2 Lithography Manufacturing Results

As a result of micro-production, Si rubber (HS II Base and Silastic 81 NW, Dow Corning) negative molds are shown in Figure 3.5. The mold in Figure 3.5(a) is used for Polydimethylsiloxane (PDMS) pouring and the one in Figure 3.5(c) is used for Polyurathyene pourin. Figure 3.5(b) and Figure 3.5(d) shows these molds SEM figures. Respecting to SEM images dimentions, molds aspect is near to the mask aspect ratio.

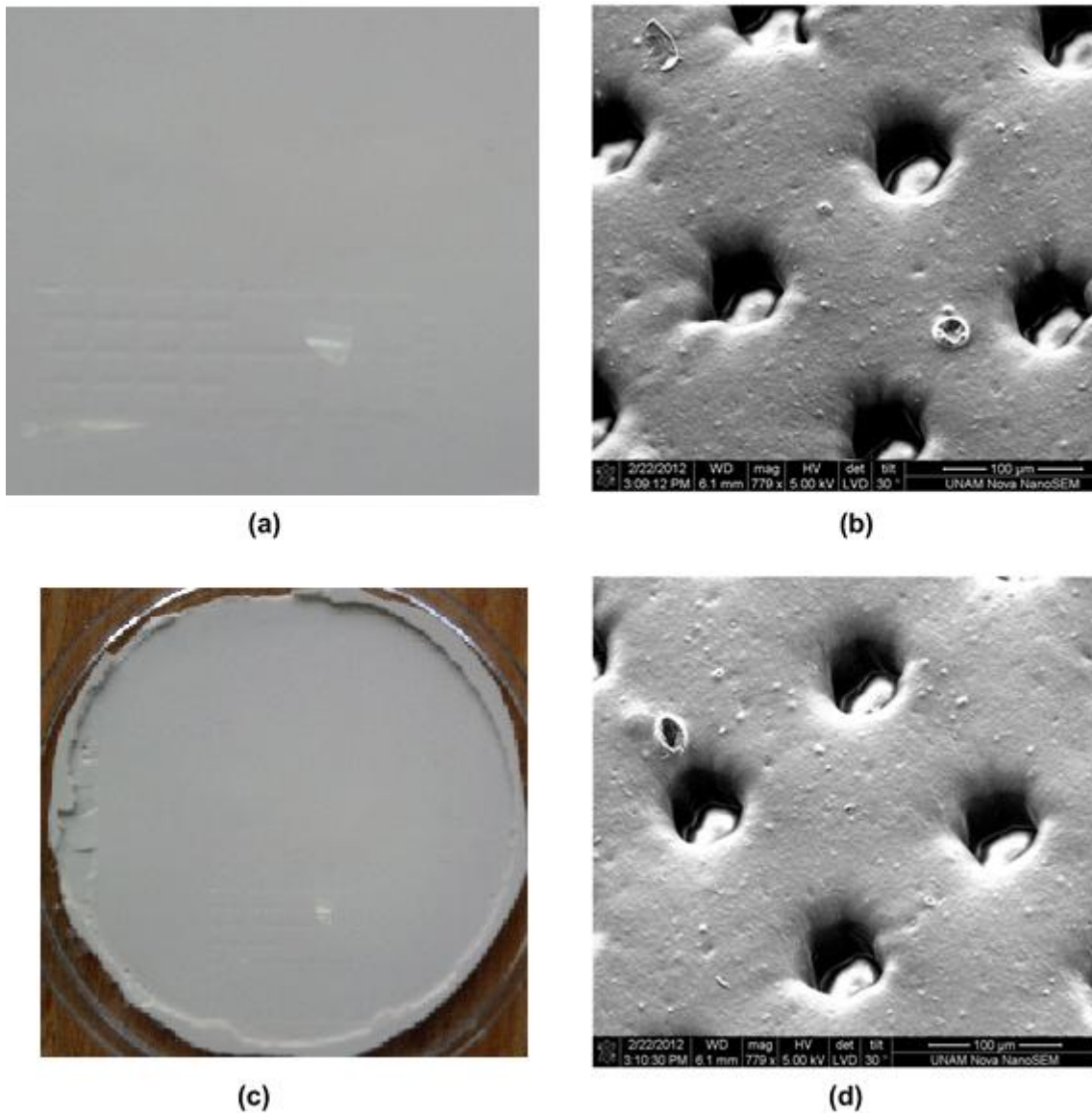

(a)

(b)

(c)

(d)

Figure 3.5 a) Si-rubber mold used for Polyurathyene pouring, b) SEM image of the mold used for Polyurathyene pouring, c) Si-rubber mold used for PDMS pouring, d) SEM image of the mold used for PDMS pouring.

As shown in Figure 3.5 polyurethane (St-1060, BJB) and polydimethylsiloxane (PDMS) (Sylgard 184, Dow Corning) is poured on Si rubber molds. St-1060 polymer base and the catalyst (A/B) are mixed with ratio of 100/55. For PDMS base and the catalyst (A/B) with ratio of 10/1 are mixed. The most important point which should be aware of in polymer preparing process is to bleed the air of prepared solution and consequently omitting the air bubbles in cured structure. For this purpose prepared polymer solution in placed in vacuum approximately for 20 minutes in 200 mTorr. Then after making sure that there is no air bubble, it is brought out of vacuum and is poured on the mold.

After a day at room temperature and following 16 hours at 70°C St-1060 polymer was cured. PDMS was cured in 24 hours at room temperature and approximately 2 hours at 70°C. Then, pealed Si rubber structure is fiber array. Figure 3.6 shows polyurethane pouring results. In Figure 3.6(a) polyurethane fiber arrays obtained from negative mold is shown. Image in Figure 3.6(b) shows front view of these fibers captured by 10x optic microscope. Images in Figure 3.6(c) and Figure 3.6(d) shows two different polyurethane fiber array obtained by two different pouring captured by 10x optic microscope. Accordingly as it is obvious in Figure 3.6(c), on the fiber array there are completely cured or wrongly cured areas. Its reason is heating St-1060 polyurethane suddenly in high temperature and do not leaving it to cure slowly before. The mold in Figure 3.6(d) is kept at room temperature for one day and then at 70°C for 16 hours on hotplate. There is no defect in Figure 3.6(d).

(a)

(b)

120 μm

(c)

0.5 mm

(d)

0.5 mm
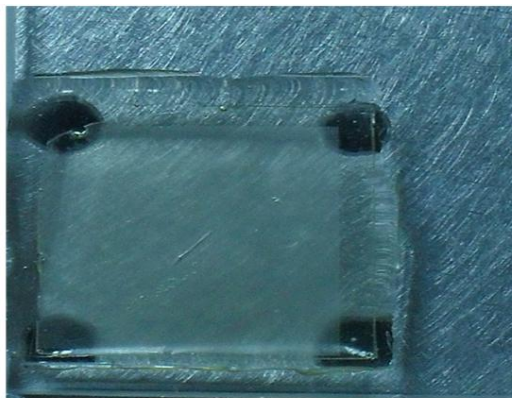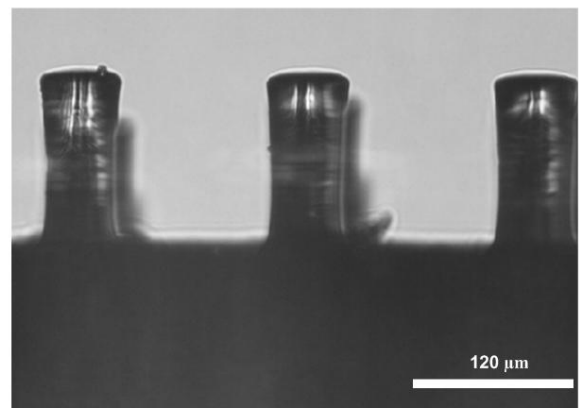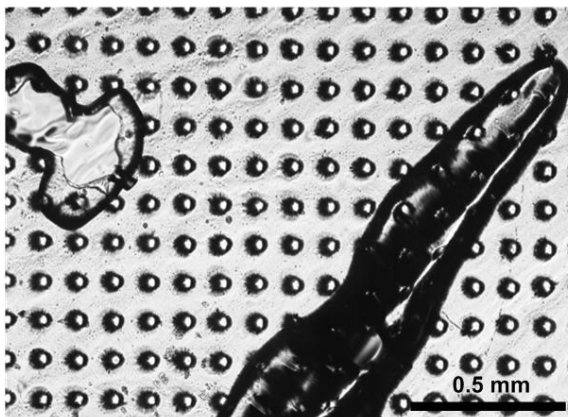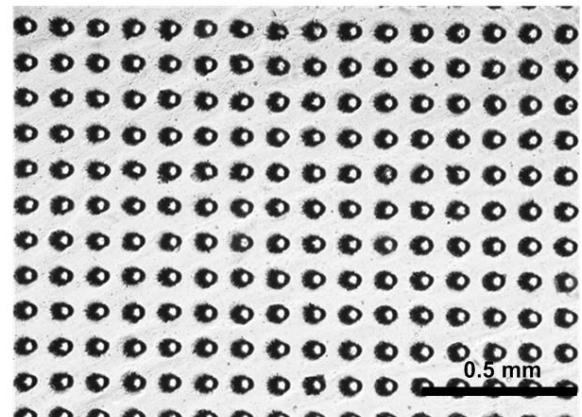
Figure 3.6 a) Polyurethane fiber array, b) Front view of fibers captured by optic microscope, c) Top view of defective polyurethane fiber array captured by optic microscope, d) Top view of the perfect polyurethane fiber array captured by optic microscope.
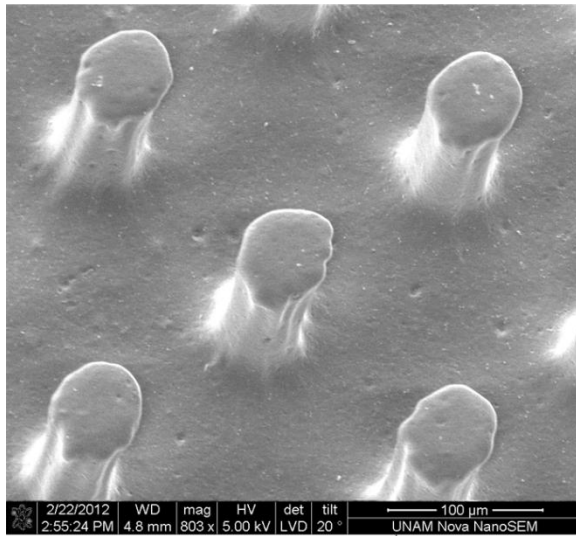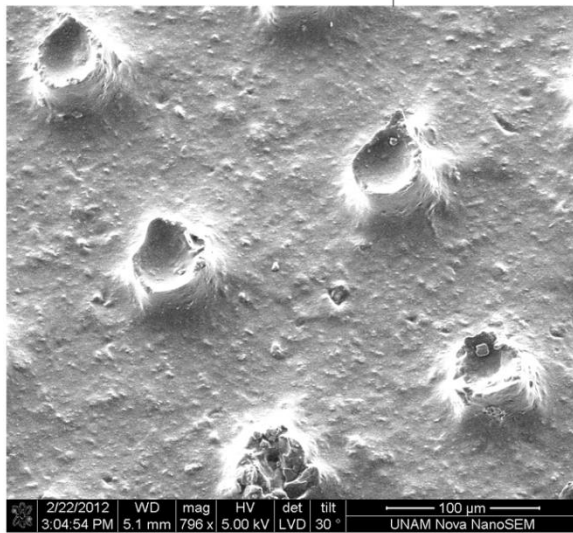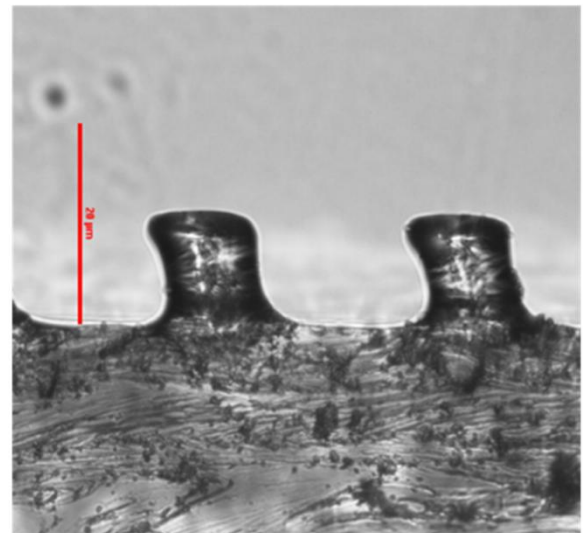
Figure 3.7 a) SEM image of polyurethane fiber array, b) Near view of SEM image captured from polyurethane fiber array, c) SEM image of PDMS fiber array, d) Microscope image of PDMS fiber array.

SEM images of fiber arrays in Figure 3.6 are shown in Figure 3.7(a) and Figure 3.7(b). Geometric properties which were defined in lithography process are observed on fibers. Despite of it, there are some problems in fiber unity. Accordingly fibers that were expected owe cylindrical figure did not result cylindrical and the fiber end is not completely circular. Because of that the parameters relating curing (temperature and time) are changed and more experiments are done. Figure 3.7(c) shows PDMS pouring SEM images. It is

23

abvios that PDMS polymer is not cured in negative mold. Figure 3.7(d) shows PDMS fibers that were poured on other mold. It is obvious that fibers height is not sufficiently high. The reason of this is supposed to be inadequate wetting of PDMS on Si rubber. To solve this problem in next step oxygen plasma is applied on the mold material and a SiO_2 (monolayer film) layer is made on the surface, and then the surface energy is increased.
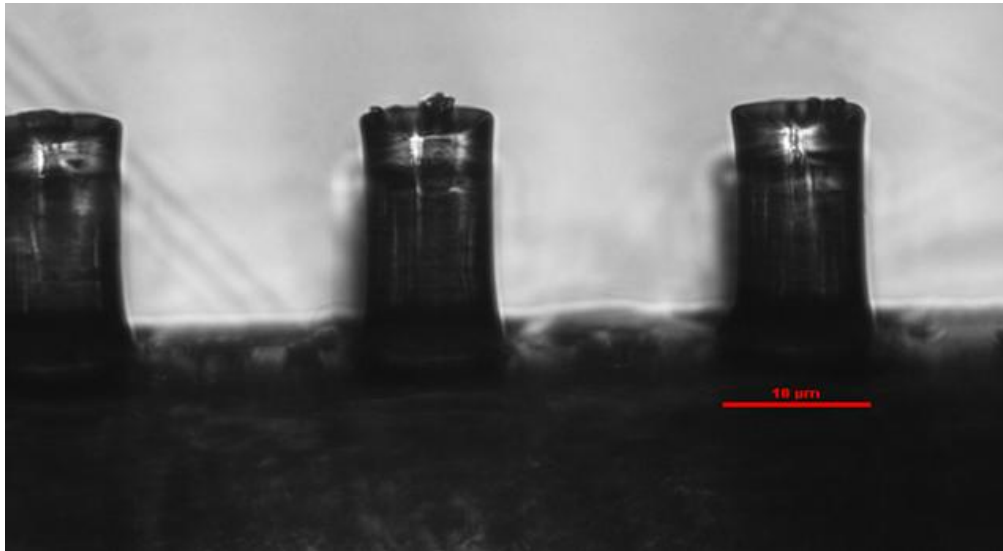
Figure 3.8 Polyurethane fiber array.
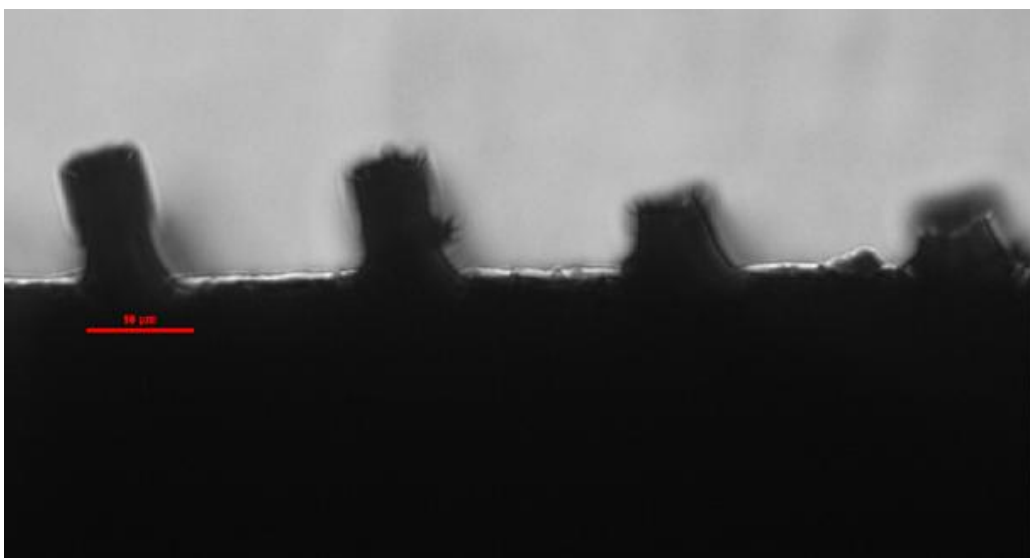
Figure 3.9 Deflected polyurethane fiber array.

4. Roughness

Characterization of surface topography is very important in applications including contact mechanics. Nearly all surfaces despite of their smooth view are microscopically rough. Surface roughness can be a result of machining or any other manufacturing processes on specimen. In modern technologies and MEMS, characterization of surface has a notable importance because of its effect on various critical physical factors [27] [28].

Generally rough surfaces can be divided into deterministic and randomly rough surfaces. Deterministic rough surfaces have inscribed shapes, like triangle or sinusoid. On the other hand, randomly rough surfaces have a pertaining to a random process which can be characterized by probability theories [29].

In this chapter roughness modeling in MATLAB is performed to use in the next chapter in contact simulations of rough surfaces with fiber arrays. Furthermore how real rough surfaces using aluminum pieces were fabricated experimentally is described to. Rough aluminum pieces are used in contact experiments which are described in next chapter

4.1 Measurement Methods

In recent years several methods have been developed to measure the roughness of surfaces. These methods can be classified in destructive or nondestructive, contacting or not. The sensitivity is another category to classify the measurements too.

4.1.1 Stylus Tools

Stylus tools working principle is based on the moving an inspector through a surface to develop the variation of height as a function of distance [30].

There are several methods to receive the vertical displacement of stylus and record the profile. One of the early methods was recording the profile on a smoked-glass plate which is shown in Figure 4.1.
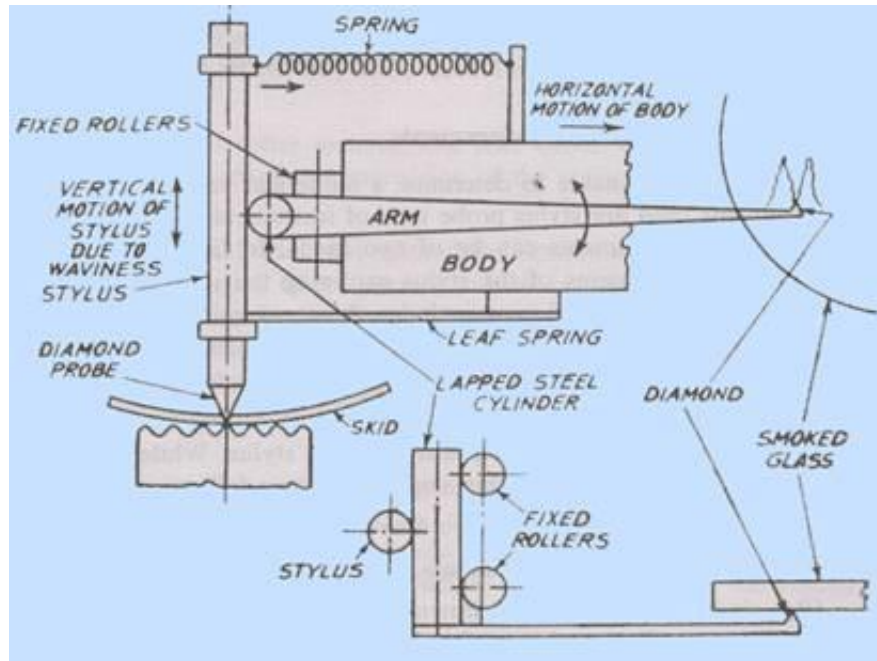
Figure 4.1 Tomlinson Roughness Meter [30].

More developed method is unifying a transducer to stylus, which converts the vertical displacement of stylus to electrical signals. Signals can be processed by computers and extract the rough surface.

Transducer which is employed in system directly affects the tool performance. Usually in cheap tools a piezoelectric crystal is used. Resolution of stylus tool depends on the manufacturer and its quality.

Roughness measurement by stylus would have errors which there are various reasons for it. Factors which lead to these errors can be stylus speed, load and size.

Exceeding stylus speed might cause stylus to lose contact with surface which happens seldom.

Applying loads more than recommended standards may cause plastic deformations on rough surface.

In Figure 4.2 effect of stylus size is shown.
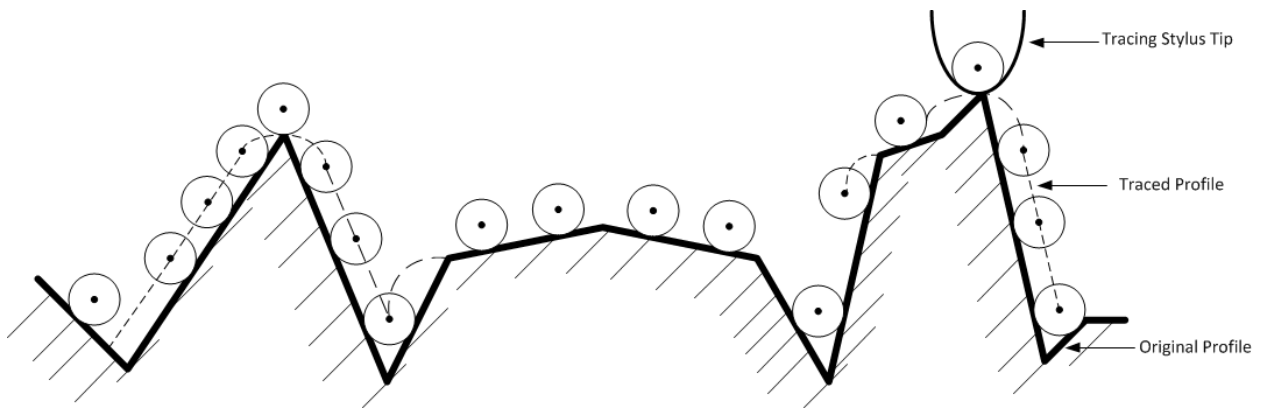
Figure 4.2 Deformity of a rough surface due to stylus size [30].

It is obvious in Figure 4.2 that the curvature of peaks and valleys or the slopes of lines are affected by the size of the stylus.

4.1.2 Optical Tools

A beam of electromagnetic radiation can be reflected off a surface in three different ways: specularly, diffusely, or both [30]. Figure 3 shows these phenomena.
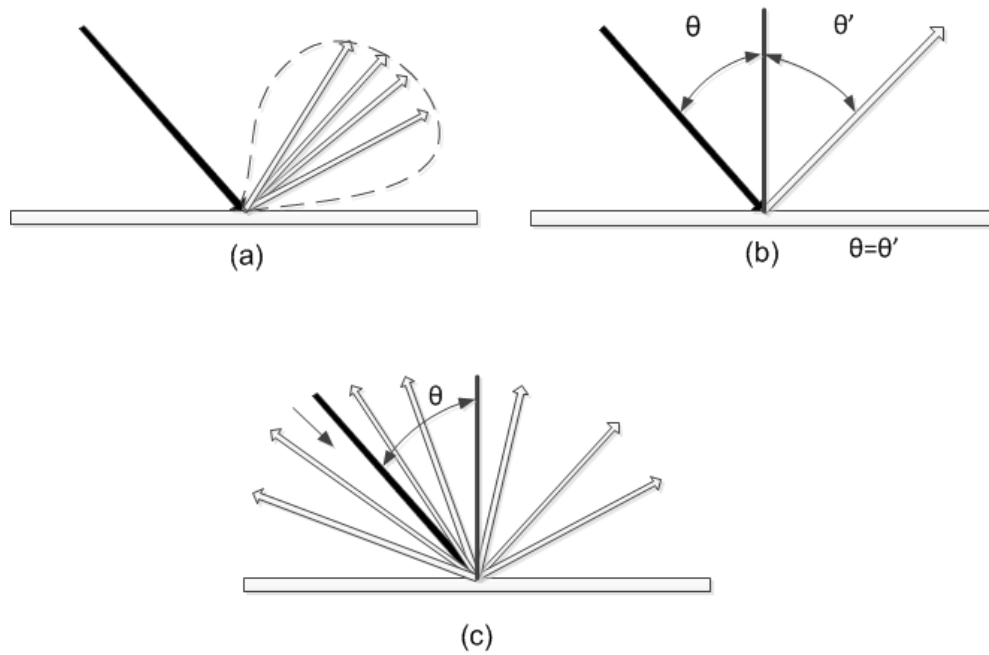
Figure 4.3 Various Reflections: (a) Unified Specular and Diffuse, (b) Specular, (c) Diffuse [30].

Dependent upon to the response of radiated beam which would be one of the above mentioned situations, roughness value of surface would be determined.

Glass meters are instruments that measure the intensity of the specular. Principle of these instruments in measuring the roughness is opposite correlation between RMS roughness and specular reflection.

Measuring the changes in polarization of a light beam that has reflected from a surface is another technique which is known as Ellipsometry [30].

Light-section microscope is another instrument that uses specular reflection. A suture image is stick out onto the surface and at the specular reflection angle objective lens captures the image. Depending on the surface, image will be straight or wavy. Straight images belong to smooth surfaces and wavy ones to rough surfaces. The working base is shown in Figure 4.4.
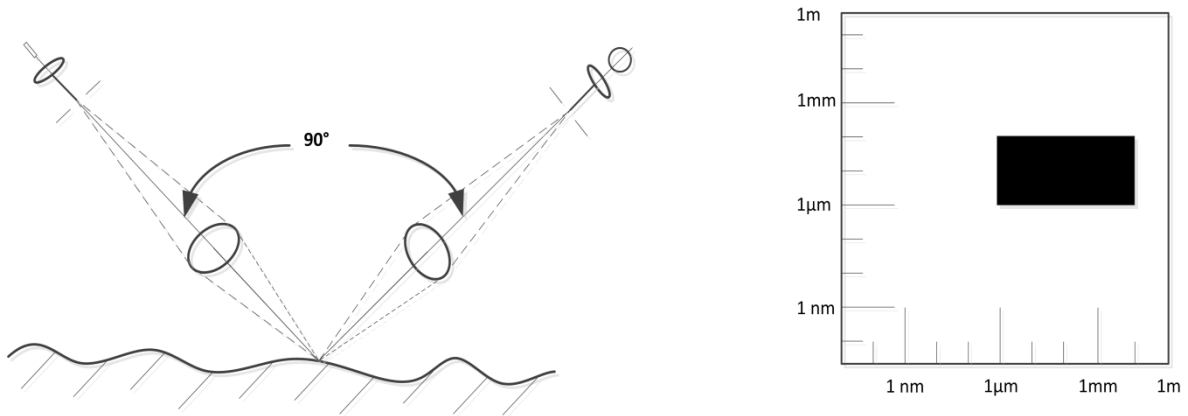
Figure 4.4 Working principle of Light-section Microscope [30].

Long-path length optical profiler instrument uses interaction of polarized light with a surface. Using an arrangement of mirrors profiler focuses o laser beam onto a surface. The laser goes through a Wollaston prism that polarizes the beam into two orthogonal components. These beams are focused on the surface and reflected back to the prism. Reflected beams is led to a beam splitter, which send every beam to various detectors. The phase difference of the polarized beams, which is related to the height difference at the surface, concludes in a voltage difference that can be measured [30]. In this work roughness is measured by optic profilometer which is described in experiments section in this chapter.

4.2 Modeling of 1-D Rough Surfaces

There are different mathematical methods to represent surfaces we face. Rough surfaces have certain mathematical properties which can be recognized by various mathematical methods [31].

Mathematically, a random rough surface can be illustrated as $h = h(r)$, where h is surface height of a rough surface with respect to a smooth reference surface, and r is the position vector on the reference surface [27].

R_a is the interface width, or RMS roughness, defined as

$$R_a = \int_{-\infty}^{+\infty} (h - \bar{h})^2 f(h) dh \qquad (4.1)$$

Another factor to define the surface roughness is R_{ave} , the average roughness , which is defined as the arithmetic average of height h,

$$R_{ave} = \int_{-\infty}^{+\infty} | h - \bar{h} | f(h) dh \qquad (4.2)$$

It is very important to select an auto-correlation function to illustrate the surface roughness. In randomly rough surfaces usually Gaussian function is used as auto-correlation function. Other functions like Setch, Lorentzaian, Bessel, and self-affine functions are also used.

Using Gaussian function to characterize a random rough surface HDF (height distribution function) is like [32] ,

$$h(r) = \frac{1}{\sqrt{2\pi\sigma^2}} \exp\left(\frac{-r^2}{2\sigma^2}\right) \qquad (4.3)$$

Where σ^2 is the variance (rms) which describes how concentrated the roughness distribution is around its mean.

Furthermore, distribution of the hills and valleys in flank face is defined by ACF (auto covariance function) like[32]

$$C(r) = \exp(-\frac{r^2}{\tau_r^2}) \qquad (4.4)$$

where τ_r is the typical distance between two point with similar specialties (correlation distance).
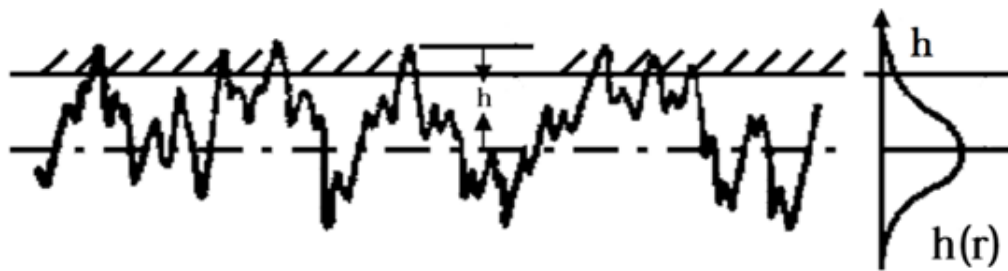
Figure 4.5 Gaussian distribution of the rough surface height [33].

4.3 Simulation of Rough Surfaces

A method which has drafted by Garcia and Stoll is employed to generate and model random rough surfaces with Gaussian distribution function [34, 35]. A random number generator is used to roll an uncorrelated distribution of surface points with a Gaussian filter to achieve correlation. Using Fast Fourier Transform (FFT) algorithm, which is based on FFTW library in MATLAB, this rolling is done [36].

Rough surface's point number, length, RMS height and correlation length should enter in code and the appropriate rough surfaces will be generated. Entering 50 points, 680e-6 length, 5e-6 RMS height and 2e-5 correlation length a rough surface has been generated as shown in Figure 4.6.
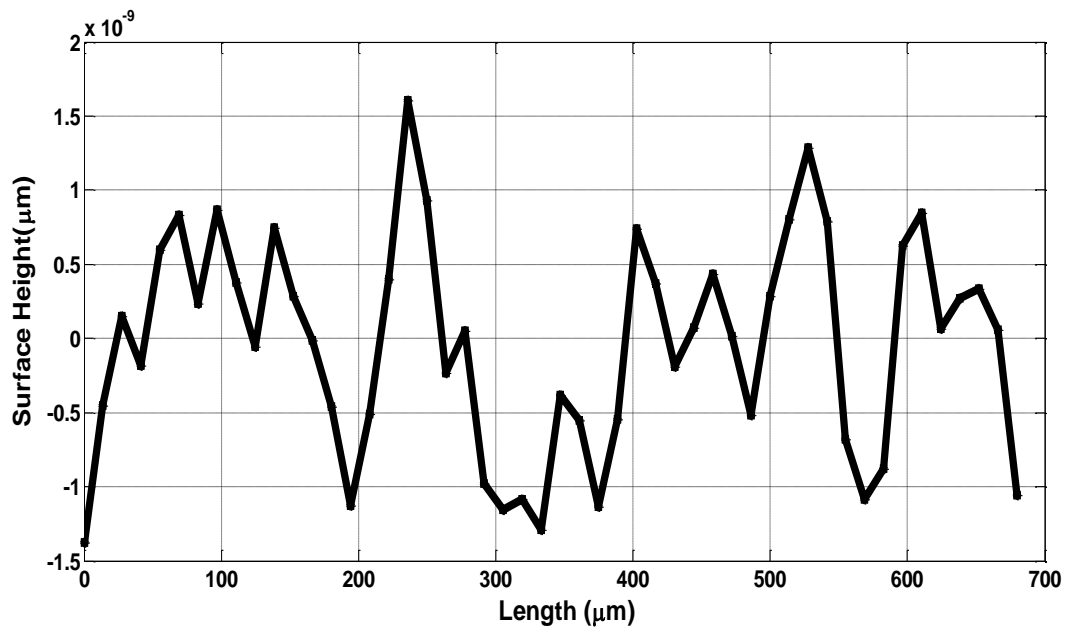
Figure 4.6 Generated rough surface in MATLAB.

The rough surface which has generated here is transported to COMSOL to perform simulations.

4.4 Experiments

Generating rough surface for experiments is an important part of the work. Aluminum is selected as the material of the rough surface. Aluminum metal sheet is cut out in 1cm × 1cm sizes. After cleaning the aluminum pieces surfaces they are rubbed by the sandpapers with different sizes. The sandpaper sizes are P400, P600, P800, P1000, P1200 and P2000, which the biggest number is the smoothest one and the lowest number is the roughest one.

Specimens are rubbed three times by each sandpaper. For the example to reach the roughness of the sandpaper number P800, orderly it is rubbed three times with every sandpapers of P400, P600 and P800. Consequently a set of different rough surfaces are obtained by rubbing Al pieces on sandpapers with different grit sizes. Figure 4.7 shows the optic microscope images of the rubbed aluminum pieces.
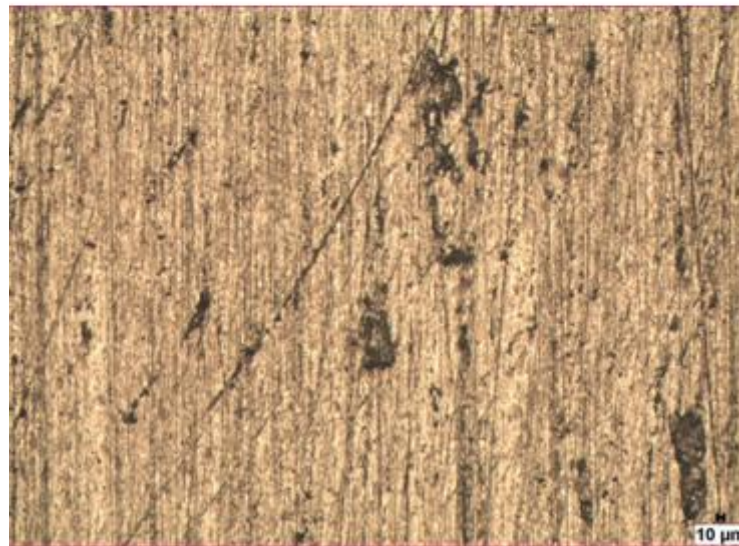
Figure 4.7 Optic microscope images of generated rough surfaces, (a) P400, (b) P1200.

Roughness value of the generated rough specimens is measured by an optic profilometer. Specimen is put on the stage of the profilometer and device is measured RMS value of the specimen. The resulting roughness values are measured to be as described in Table 4.1. The profilometer which is used to measure RMS values is shown in Figure 4.8.

Sandpaper No.	RMS value
P400	1.62
P600	0.97
P800	0.87
P1000	0.72
P1200	0.47
P2000	0.19

4.1 RMS values of specimens.

Figure 4.8 Zygo- Newview 7200 optic profilometer (NNRC).

5. Contact Mechanics

Examining several branches of Solid Mechanics will result us that a wide area of solid bodies are under pressure loads which results contact studies around it. Studying the deformation of solid bodies which touch each other at least in one point is Contact Mechanics. Contact Mechanics is studied by mechanics of material and continuum mechanics. Elasticity, viscoelasticity and plasticity are taken in account in studies. The most important factors that are studied consists strain, stress and adhesion forces during any contact. Stress concentrations are important as they are the failure sites in body. Current studies are widely focused on micro and nanotechnology [37] [38].

The perpendicular stresses and adhesion to the contact bodies are in the center of the attention. They play the main role in examining the failure and pull off forces in contact [39].

In other hand, real contacting surfaces are rough and there in no pure surface without any roughness. Herewith the contact always occurs between rough surfaces and the analyses should involve rough surface analyses too. In rough contacting surfaces contact is occurred in a bunch of microscopic actual contact areas. Here all of the results will be different with pure surfaces [39].

In 1882 Heinrich Hertz published 'On the contact of elastic solids' paper which is considered as the base of the contact mechanics. Hertz was working on optical lenses. He was researching that how does the optical properties of lenses can change by forcing them together and contact them each other. He got that if two curved surface come together and deform each other under load the resulted stress would depend on normal contact force, the elasticity of both bodies and radius of curvature of both bodies. Effect of geometrical factors is obvious. In this theory any surface interactions such as van der Waals interactions or contact Adhesive interactions are ignored [39].

In 1970 Johnson et al. improved the Hertzian theory. Although Hertz does not involve adhesive in account in contact but JKR (Johnson, Kendall, Roberts) theory

did it. Then as a result, the contact will be formed during unloading regime too. In other words we would be able to study the contact in pulling mode too. JKR-theory is restricted to the sphere-sphere contact similarly to the Hertz theory.

The DMT theory is more involved theory which considers van der Waals interactions outside the elastic contact regime, which adds one more load. This theory surveys the Bradley's van der Waals model of two separated surface in which the deformations concluded by attractive interaction forces are ignored [40] [39] [37].
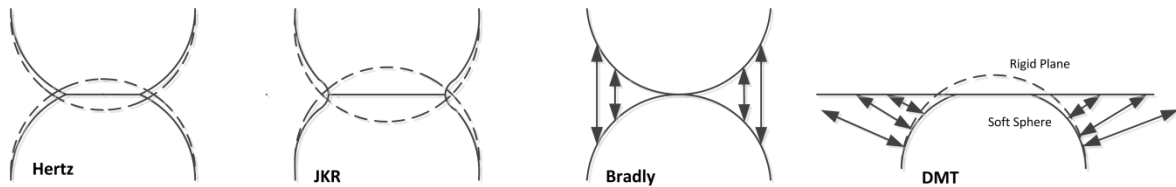
Figure 5.1 Mechanical contact models: Hertz: fully elastic model , JKR: fully elastic model considering adhesion in the contact zone, Bradley: purely van der Waals model with rigid spheres, DMT: fully elastic, adhesive and van der Waals model [37].

In this work the fibrillar structures is gone under contact with smooth and rough surfaces.

5.1 Formulation

The problem is considered in elastic regime. A fiber with radius of r and height of l is considered as shown in Figure 5.2. The fiber is on its backing layer and from its top is bonded to a rigid substrate. A displacement of Δ is applied to rigid substrate. Consider P is the applied force on fiber resulting from displacement of Δ. For very long fibers P is proportional to the strain like [41],

$$\varepsilon = \Delta/l \qquad (5.1)$$

$$P = E \frac{\Delta}{l} \pi r^2 \tag{5.2}$$

where E is the Young modulus of fiber. If fiber gets shorter its condition is changed and shows some different behavior of fibrillar specialties. Studying this condition gives us P for shorter aspect ratios like,

$$P = E \frac{\Delta}{l} \pi r^2 \, n\left(r/l\right) \tag{5.3}$$

where n is a function of dimensionless parameter of r/l. n can be explained as the stiffness ratio of a fiber with aspect ratio of l/r to that has an infinity length.
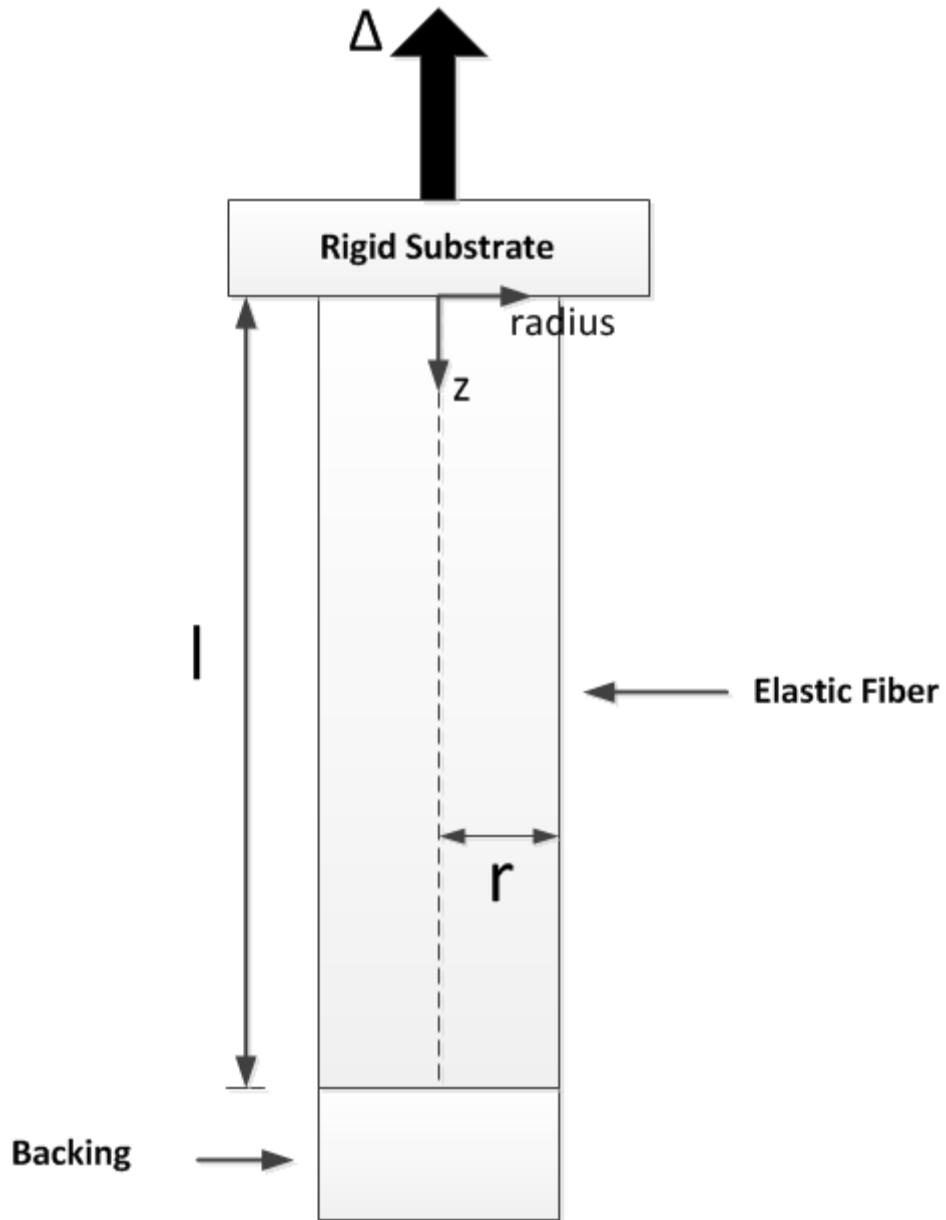
Figure 5.2 Elastic fiber contacting a rigid substrate.

The stress near the edge of fiber is,

$$\sigma(z = 0, radius \rightarrow r) = Q(radius - r)^{-\lambda} \qquad (5.4)$$

where λ, which changes between 0-1 and depends on Poison ratio of fiber, is approximately 0.4 for $\nu=0.5$ [42]. In equation above Q represents the amplitude of the singular stress of fiber. Amplitude Q is given by,

$$Q = E \frac{\Delta}{l} r^\lambda j \left(\frac{r}{l} \right) \tag{5.5}$$

where j, just depends on r/l and is a dimensionless factor. In general it is unknown but as r/l approaches to zero equation above becomes like,

$$Q = E \varepsilon r^\lambda j(0) \tag{5.6}$$

Failure occurs as the amplitude of singular stress (Q) reaches a critical value. As Q gets its critical value, Q_c , a crack between fiber and rigid substrate occurs and starts to propagate until the failure occurs. Using Equation (5.2), Equation (5.5) pull-off force can be determined as following equation,

$$P_f = \frac{\pi Q_c r^{2-\lambda}}{j(r/l)} n(r/l) \tag{5.7}$$

The ratio of n to j is defined as s,

$$s\left(\frac{r}{l}\right) = \frac{n\left(\frac{r}{l}\right)}{j\left(\frac{r}{l}\right)} \qquad\qquad (5.8)$$

Tang et al extracted Q_c value. They used Dugdale-Barenblatt (DB) model to model the failure between fiber tip and substrate [42, 43]. Their model describes the interfacial adhesion between fiber and adhering substrate. This model assumes that the interface fails when the tension stress (σ) in the cohesive zone reaches the intrinsic strength of the contact (σ_o). Therefore, the crack initiates and propagates whenever the maximum stress reaches a certain value. The ratio of (σ/σ_o) depends on a dimensionless parameter (χ) such as [41, 42]:

$$\sigma/\sigma o = \begin{cases} B\chi^{-\lambda} & \chi \gg 1 \\ 1 & \chi \ll 1 \end{cases} \qquad\qquad (5.9)$$

$$\chi = \frac{\sigma_0{}^2 r}{2\pi E^* W_{ad}} \qquad\qquad (5.10)$$

where, $E^* = E/(1 - v^2)$, E is the elastic modulus of the fiber, W_{ad} is the work of adhesion, B is a numerical constant. In the DB cohesive zone model, work of adhesion is simply the multiplication of intrinsic strength and critical separation length (δ_{cri}) ($W_{ad}=\sigma_o \delta_{cri}$).

5.2 Finite Element Analyses

Finite element simulations are conducted to see the effect of roughness on the adhesion of fibrillar features to the surface in the elastic regime. In terms of adhesion, there exist two competitive processes when a fiber array comes into contact with a rough surface. First one is the enhancement of the adhesion due to the apparent contact increase (compliance) and second one is the decrease of adhesion due to the elastic energy release in the contact area. In the simulations,

a rigid rough surface put into contact with a fiber array to observe stiffness and pull-of stress value using the elastic constants and interfacial adhesion.

For simplicity of analysis, one dimensional rough surface is generated using the Gaussian distribution and based on the model derived by Stoll et.al. cite [34, 35] which is completely described in chapter 4. One dimensional rough surface is imported into the commercially available finite element software COMSOL MultiPhysics. The rough surface is generated with treating each data points as the key points and unified using the Bezier curve as seen in Figure 5.3(b).
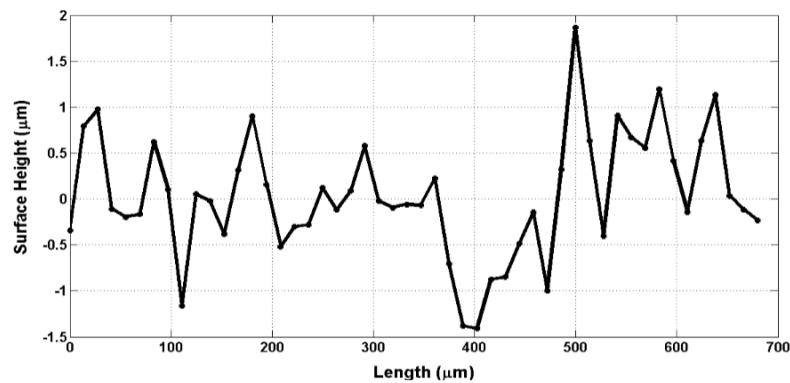
(a)
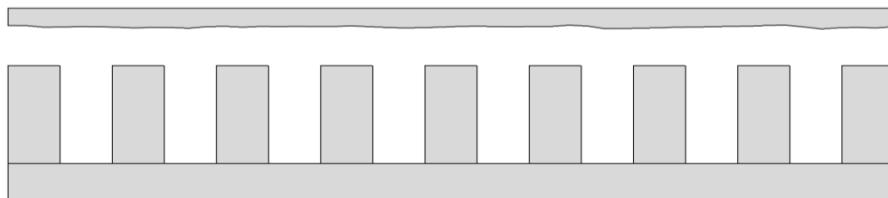
(b)

Figure 5.3 a) One dimensional rough surface data points, (b) rough surface and fiber array are shown.

The simulations are carried out by applying a harmonic displacement to the rigid rough surface in the vertical direction (Figure 5.5). Fiber array with backing layer consists of 9 cylindrical elastic fibers. It is fixed from the bottom part while the rigid surface brought into contact with the fibers applying a preload value. After the

specified preload is reached, the rough surface is retracted back in order to determine the stiffness and pull-off force of the fiber array. Meshing is done by Physics-controlled mesh command. As this command is selected COMSOL Multiphysics creates a mesh that is adapted to the current physics settings in the model. In our simulations Triangular elements are selected. Table 5.1 shows meshing details of simulations. The cohesive model of Dugdale-Barenblatt (DB) is implemented for each soft elastic cylindrical fiber contact with the rigid rough surface in order to account the interfacial adhesion [42, 43]. This model assumes the interface fails when the tension stress (σ) in the cohesive zone reaches the intrinsic strength of the contact (σ_o) as explained in formulation section.
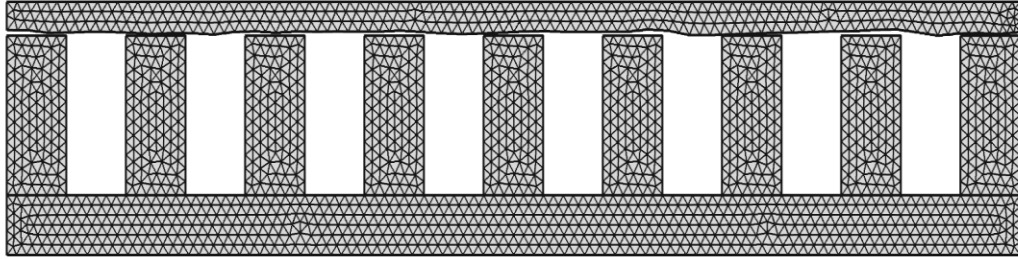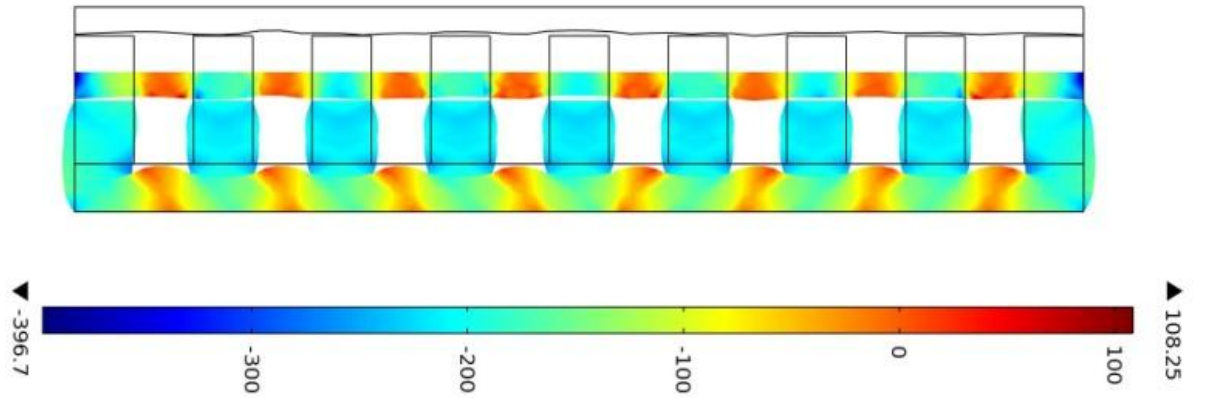
Figure 5.4 Meshing.

(a)
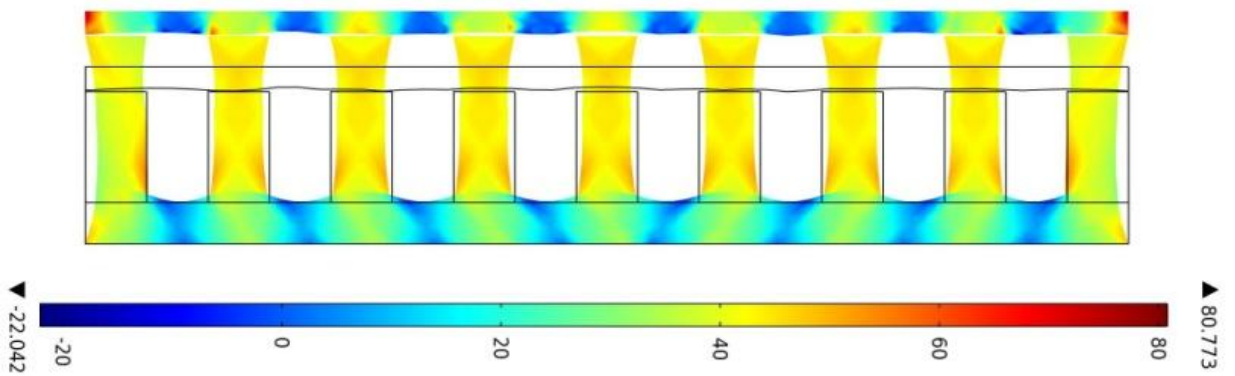
Figure 5.5 (a) Pushing rough surface on micro fibers, (b) pulling over rough surface.

Feature	Value
Triangular Elements Number	**3561**
Edge Elements	**687**
Vertex Elements	**90**
Minimum Element Quality	**0.8634**
Average Element Quality	**0.9819**
Element Area Ratio	**0.2899**
Mesh Area	**5.961e-8 m^2**

5.1 Meshing features of simulations.

The simulations are carried out by controlling the displacement for various aspect ratios. Each fiber diameter is taken as 40 µm, backing layer thickness is 30 µm, lateral dimension is 680 µm and E is taken as 1.8 MPa. X value in simulations is 30 and n,j and s values are calculated using simulation results. The stiffness value is calculated by extracting pressure integral using the contact boundary while applying predefined displacements to the rough surface. Stiffness is evaluated for various contact surfaces with different rms values. Figure 5.6 shows stiffness change with respect to radius/length ratio change.   Similarly, pull-off force is calculated using the same method. Pressure is modified to force after extracting from simulations, and then pull-off force is calculated. The pull-off stress variation with respect to radius/length ratio change is presented in Figure 5.7.

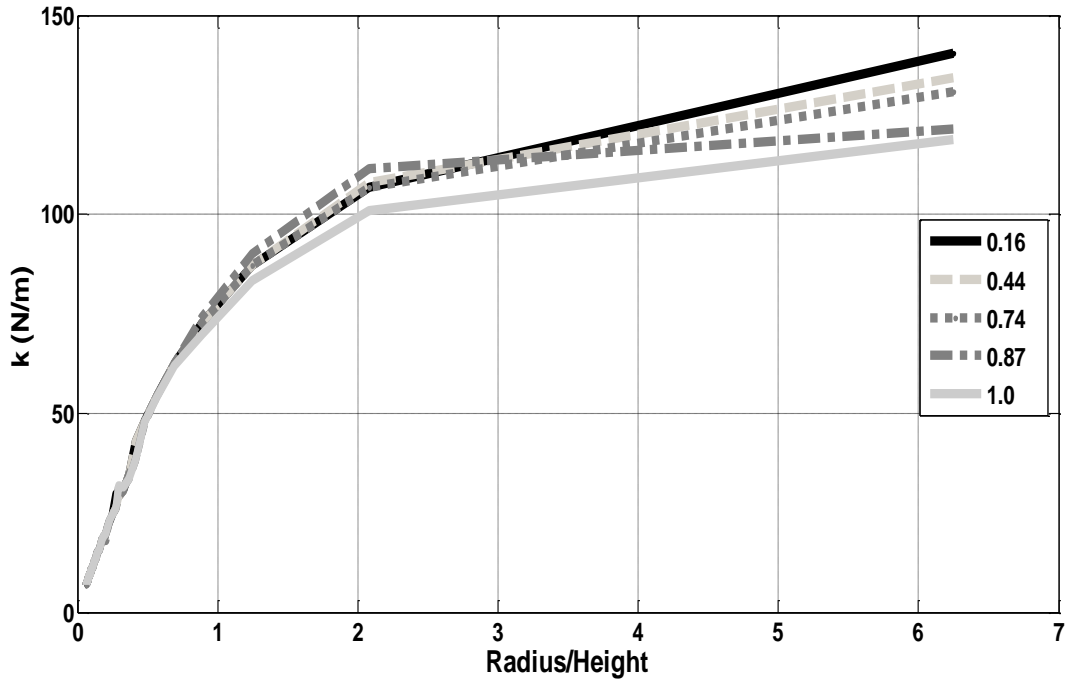**Figure 5.6** The stiffness (k)-inverse of aspect ratio (1/(AR)) graph for different rough surfaces. Inset is the rms values of the surfaces. For high aspect ratio fibers the effect of the roughness is not pronounced.
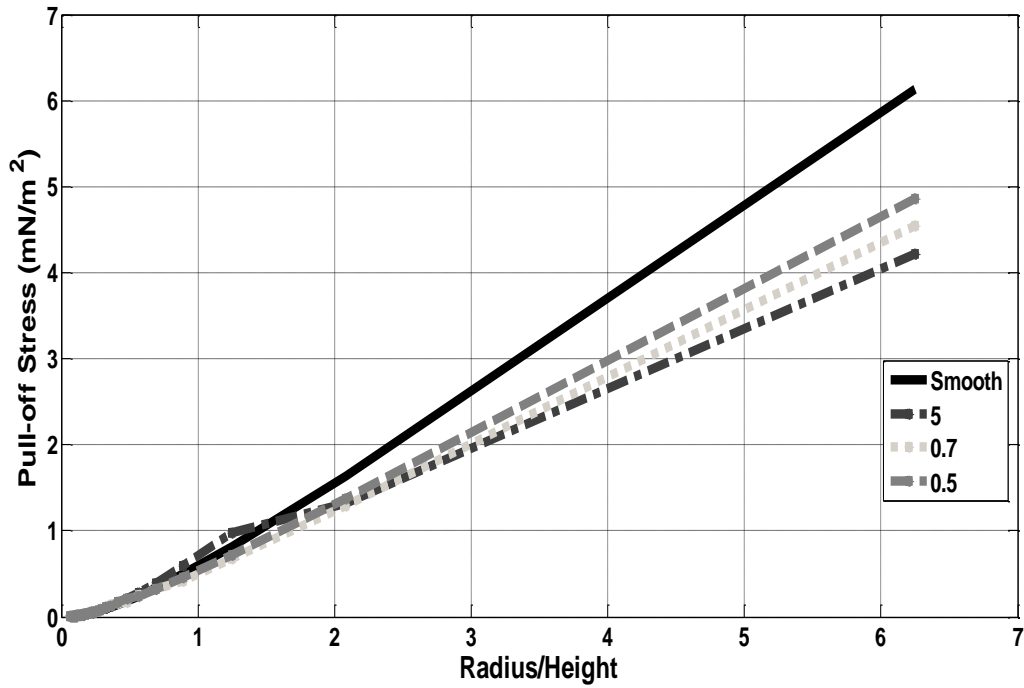

Figure 5.7 The pull-off stress (σ)- inverse of aspect ratio (1/(AR)) for different rough surfaces.

Lower aspect ratio results in a stiffer fibrillar structure as shown in Figure 5.6. Thus, the decrease of the aspect ratio makes the structure behave like a simple flat film where the compliance enhancement disappears. As the compliance decrease, the rough surface adaptation capability of the fiber array lessened. The fiber array with high aspect ratio does not affected by the roughness change as one can observe in Figure 5.6, i.e. the radius/length ratio is smaller than 1. Similarly, the pull-off force values is unaffected by the roughness change in the high aspect ratio regime (as seen in Figure 5.7). However, as the fibrillar structure converges to a flat case by decreasing the aspect ratio, the pull-off force becomes sensitive to the roughness change of the rigid surface.

5.3 Experiments

Fiber array, which is made from polyurethane, are fabricated using photolithography techniques which is detailed in chapter 3 [42, 44]. The aspect ratio is 0.63 with a diameter value as 50 μm and the height is 80 μm. The thickness of the backing layer, where the fibers stand on, is measured to be 1 mm. The fibers are packed in a square shape with overall dimensions of 1x1 cm.

The experimental setup consists of a high resolution load cell, a vertical linear stage that is connected to a controller, a signal conditioner and data acquisition system which its schematic is shown in Figure 5.8.

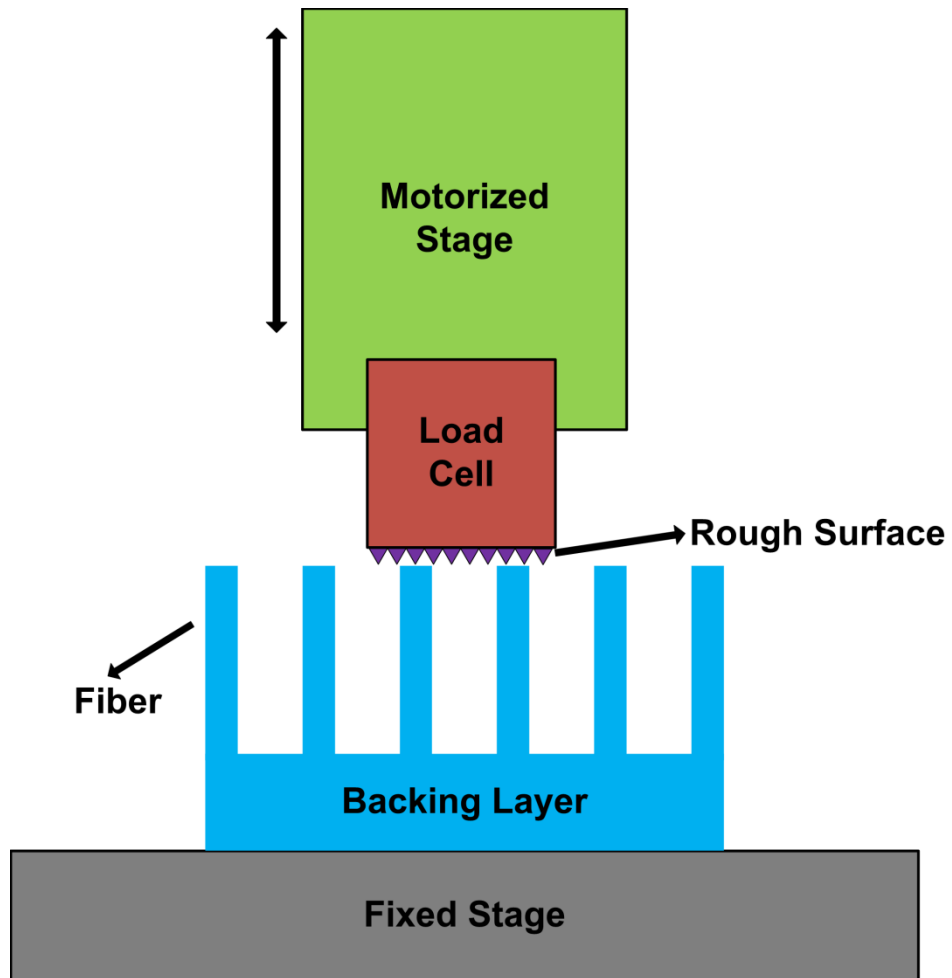**Figure 5.8** Schematic of the experimental setup.

5.4 Experiment Setup

Experimental setup is designed to test fabricated fiber arrays in contact with rough and smooth surfaces. The working schematic of experimental setup is shown in Figure 5.9.
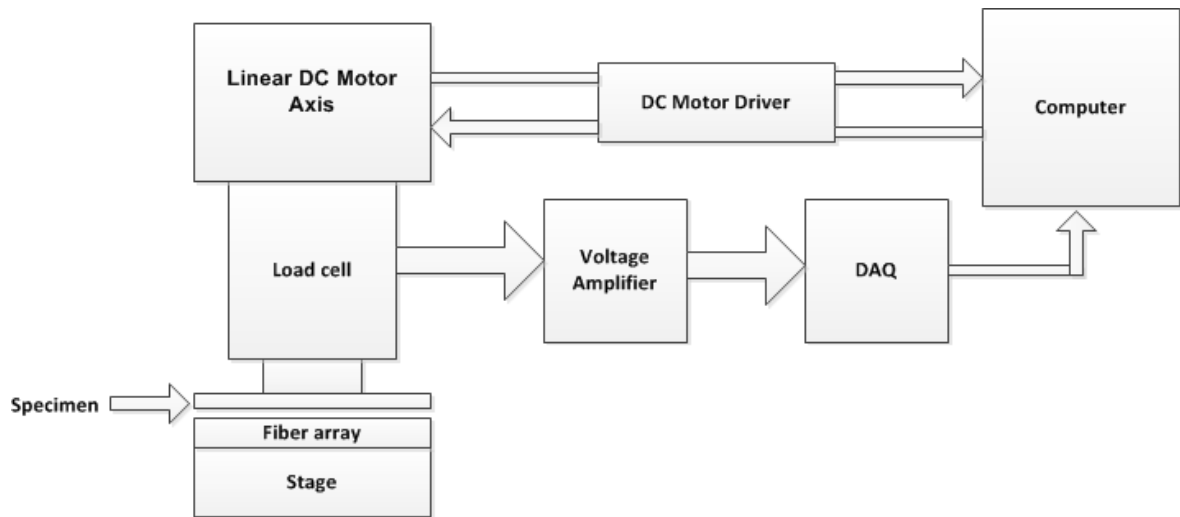
Figure 5.9 Working schematic of experimental setup.

5.4.1 The working Principle

Programming of the setup is done by LabVIEW 2009 program situated in Hacettepe University Mechanical Engineering faculty. Motion command is send to motor driver from computer and one dimensional linear motor which load cell is installed on tip of that moves toward fibers and applies them compressing force. Aluminum piece is attached to the load cell tip. Applied compressing force is considered as preload. As preload is measured by load cell, it is raised to the desired voltage value in amplifier. Simultaneously DAQ (Data Acquisition) unite modifies analog output of the load cell to digital to be readable for computer and we can see the load value simultaneously in program interface. Then depending on users desire it can stop for a while and then turn back or it can turn back simultaneously in reverse direction (up) and fibers start to pull and pull-off force is measured by load cell. Top point of the measured force values is the preload force and negative top point is the pull-off force. Figure 5.10 shows an example of Force-Time graph drawn by data extracted from an experiment.

As contact occurs between flat rough surface and fibers, during contact process some of the fibers slip and do not go under complete contact and consequently graph hill is not a sagittal in Figure 5.10.
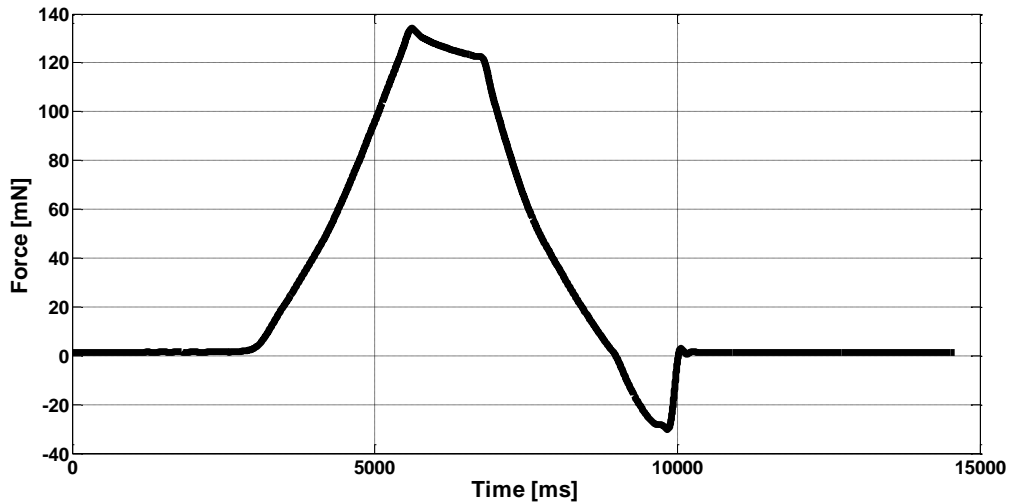
Figure 5.10 Force- Time graph.

5.5 Experiment Process

A flat sheet of aluminum (Al) with the same size of the fiber array is produced and attached to the load cell. Figure 5.11 shows the experimental setup. A set of different rough surfaces are obtained by rubbing the sandpaper on the Al plate with different grit sizes. The resulting roughness values are characterized by an optical profilometer and are measured to be as 0.19, 0.47, 0.72, 0.87, 0.97 and 1.62 μm in root mean square which has been described in chapter 4 entirely.

A custom build software is used to move the linear stage vertically with a low constant speed (V=1 μm/s). The Al sheet comes into contact with the fibers and the preload (F_{pre}) is applied to the fibers. The rough surface is retracted back after a predefined force value is attained. The maximum tension force obtained in the experiments will be taken as pull-off force (F_p) since the exact point of separation of the fibers from the surface is difficult to locate for fixed grip experiments.
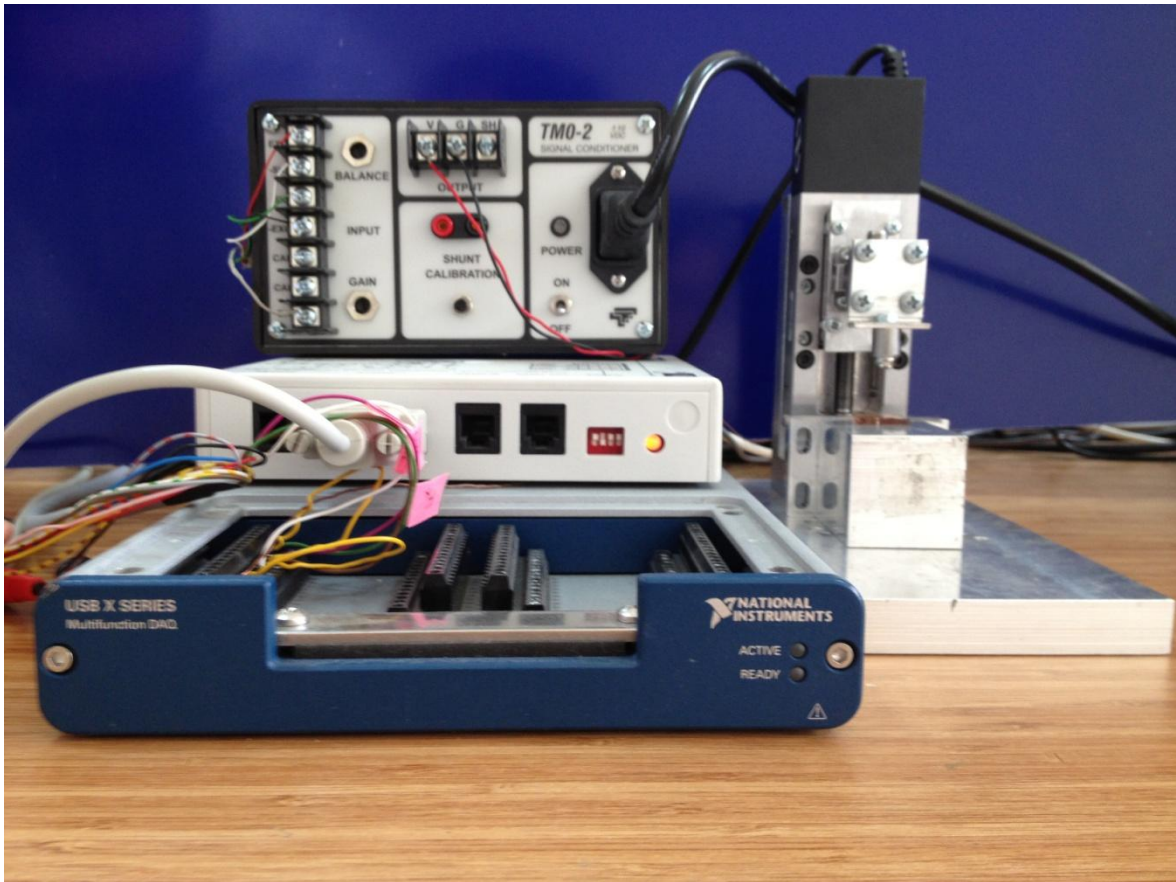
5.11 Picture of experimental setup.

Two set of experiments are performed to investigate the preload and roughness dependence of the pull-off force. In the first set of experiments, preload value is changed from 10 mN to 90 mN for a rough surface (Figure 5.12). In the next part of the experiments, rough square aluminums are brought into contact with fiber array using a constant preload value of 60 mN (Figure 5.13). Each experiment is repeated three times to account the measurement errors coming from the experimental setup.

The measured pull-off force increases with the preload force change as expected. Also, the increase of roughness of the surface leads to a decrease in the pull-off force values as predicted by the FEM simulations. There are three order magnitude differences between simulations and experimental values. This may be due to the backing layer thickness effect which has a detrimental effect on the pull-off force values. This observation is confirmed using FEM simulations as shown in

Figure 5.14. Higher backing layer thickness results in a lower pull-off force. As the backing layer gets thinner, the fibers are decoupled in terms of the crack trapping and compliance of the structure is enhanced. In contrary, increasing the backing layer thickness decrease the enhancement of fibrillar features on pull-off forces due to the structural coupling of fibers with the backing layer.
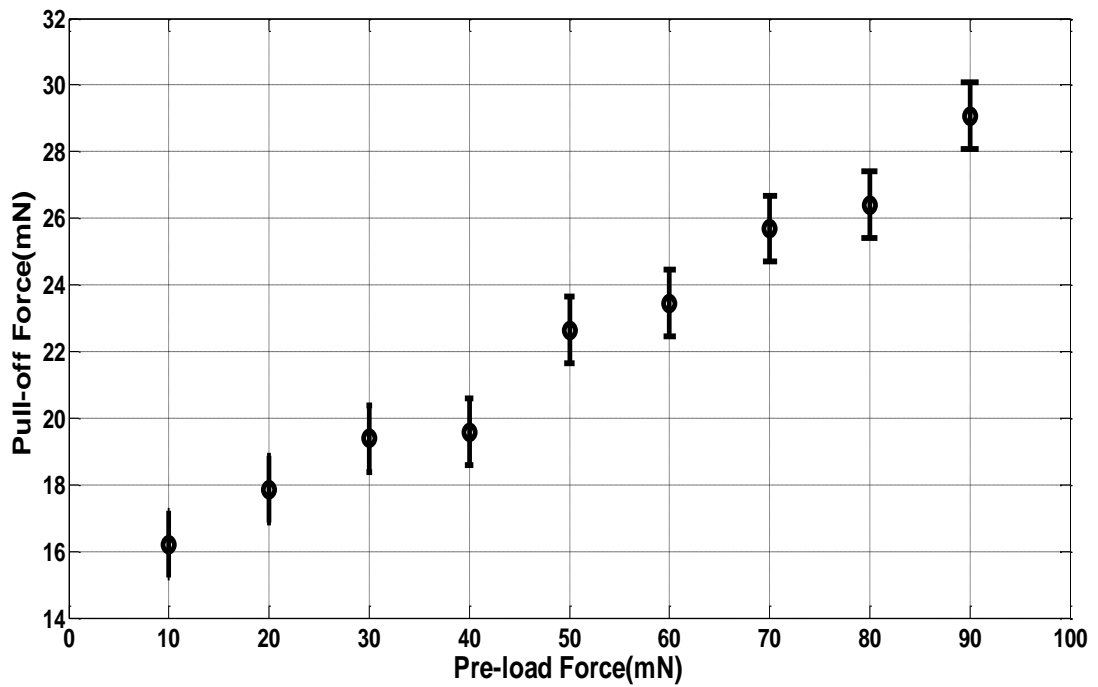
5.12 Preload force value is increased while observing the experimental pull-off force.
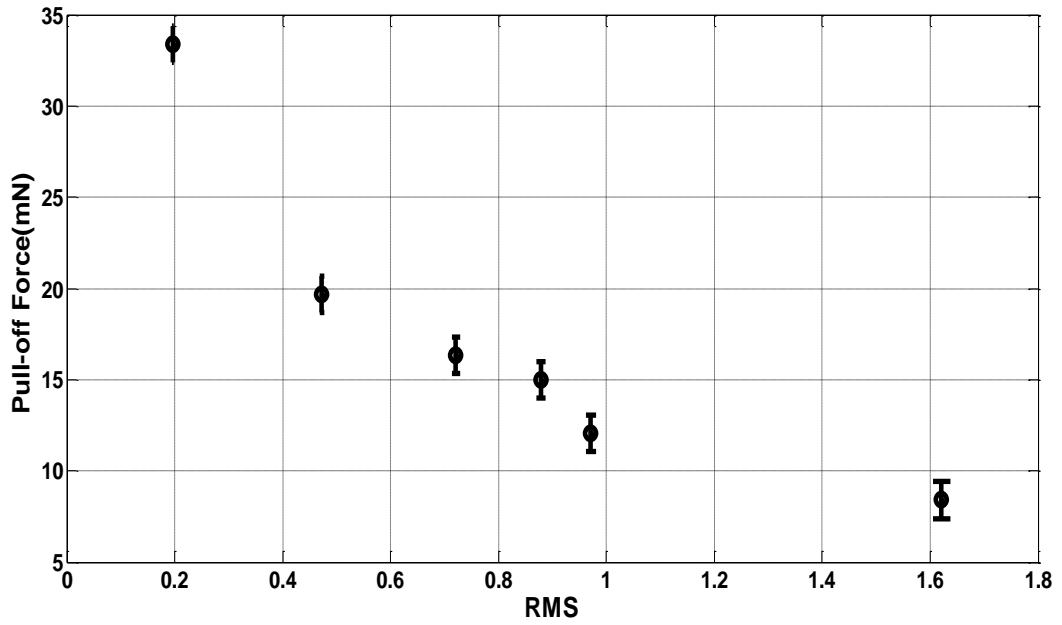
5.13 Experimental pull-off force values for different rms values.
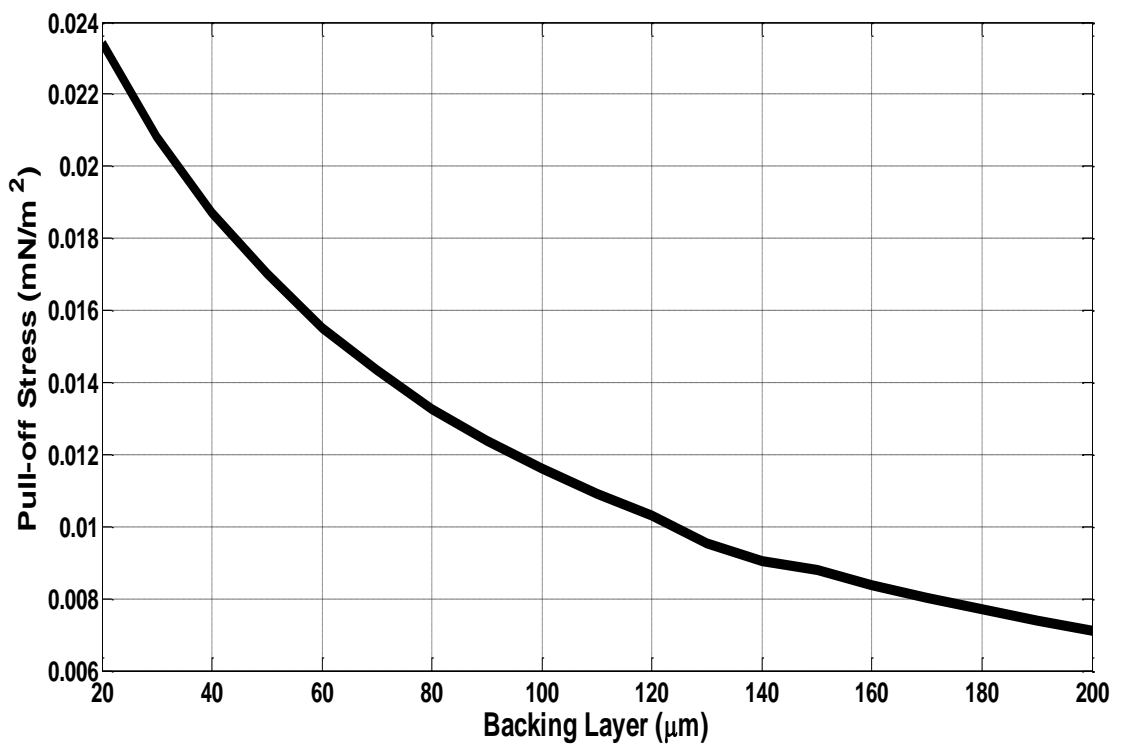
5.14 FEM simulation result for pull-off force with backing layer thickness increment.

Conclusion

To fabricate fibers with proper features, micro fiber design performed. Their failure conditions were discussed and critical design parameters were extracted. Buckling, matting and defect resistance failures examined and their failure graphs drawn. Maximum height in matting condition calculated to be 102.8 μm. the height limitation was decided respecting fiber diameter and gap between fibers.

Respecting designed parameters fabrication has been done by soft lithography method. Fabrication has been done with negative photoresist SU-8. Master molds have been achieved and fibers obtained by pouring polyurethane on molds. During spin coating applying accurate recipe is very important and after that baking time and its recipe is important to avoid any defects on the fibers. Furthermore rehydration should be enough and the developing time should not exceed proper time to result high quality fibers.

Then rough surfaces owing various RMS values fabricated. Sandpapers with different roughness values used to fabricate rough surfaces. Aluminum pieces rubbed on sandpapers and rough surfaces obtained. Using optic profilometer in UNAM, RMS values of rough surfaces measured. RMS value of specimens is in 0.19-1.62 μm interval. There are 6 various specimens. Also rough surface simulations have been done in MATLAB. Surfaces with desired RMS values have been simulated in MATLAB with specific point numbers and length.

Finally contact simulations and experiments have been done. Both fibers and rough surfaces have been simulated in commercially available finite element software COMSOL MultiPhysics. One dimensional rough surface which had simulated in MATLAB imported in COMSOL MultiPhysycs and contact process modeled. The cohesive model of Dugdale-Barenblatt (DB) implemented for each soft elastic cylindrical fiber contact with the rigid rough surface in order to account the interfacial adhesion. Simulation results showed that the decrease of the aspect ratio makes the structure behave like a simple flat film where the compliance enhancement disappears. As the compliance decrease, the rough surface adaptation capability of the fiber array lessened. However, as the fibrillar structure

converges to a flat case by decreasing the aspect ratio, the pull-off force becomes sensitive to the roughness change of the rigid surface.

Also experiments showed that the measured pull-off force increases with the preload force change as expected. Besides, the increase of roughness of the surface leads to a decrease in the pull-off force values as predicted by the FEM simulations. There were differences in magnitude of value which was considered to be related with backing layer.

References

1. Ashley, J.F.C., Neil B Davis, Robert H Bowman, Christopher N, *Soft-lithography fabrication of microfluidic features using thiol-ene formulations.* Lab on a chip, 2011. **11**(16): p. 2772-8.
2. J., B., *MEMS: a closer look at part 2: the MEMS industry in Silicon Valley and its impact on sensor technology.* SENSORS, 1996. **July**: p. 4–38.
3. Bryzek J, P.K., McCulleyW., *Micromachines.* IEEE Spectrum, 1994. **May**: p. 20–31.
4. HP, H., *Micro-Optics: El- ements, Systems and Applications.* 1997, London: Taylor & Francis.
5. Kovacs GTA, P.K., Albin M. 1996., *Silicon micromachining: Sensors to systems.* Anal. Chem., 1996. **68**: p. 407A-12.
6. WM., M., *Moreau WM.* 1998: Plenum.
7. P, R.-C., *Handbook of Microlithography, Micromachining, and Microfabrication.* Vol. 1. 1997, Bellingham: WA: SPIE Opt. Engineer. Press.
8. MD, L., *Extending optical lithography to the gigabit era.* Solid State Technol., 1995. **February**: p.:57−66.
9. Cerrina F, M.C., *A path to nanolithography.* Mat. Res. Soc. Bull., 1996: p. 56–62.
10. MD., L., *Extending optical lithography to the gigabit era.* Solid State Technol., 1995. **February**: p. 57−66.
11. L., G., *Solid State Technol.* IEEE Spectrum, 1996. **April**: p. 33-38.
12. Miller RD, W.G., *Polymeric silicon-containing resist materials.* Adv. Mater. Opt. Electron., 1994. **4**: p. 95–127.
13. Persson, B.N.J., *Sliding Friction: Physical Principles and Applications.* 2nd ed. 2000, Heidelberg: Springer.
14. B. N. J. Persson, J.C.P., *Theory of rubber friction and contact mechanics. with adhesion.* Phys. Rev. Lett, 2001.
15. Greiner, C.C., Aranzazu Del Arzt, Eduard, *Adhesion of bioinspired micropatterned surfaces: effects of pillar radius, aspect ratio, and preload.* Langmuir : the ACS journal of surfaces and colloids, 2007. **23**(7): p. 3495-3502.
16. Persson, B.N.J.T., E., *The effect of surface roughness on the adhesion of elastic solids.* The Journal of Chemical Physics, 2001. **115**(12): p. 5597.
17. Vajpayee, S.J., Anand Hui, C.-Y., *Adhesion of a Fibrillar Interface on Wet and Rough Surfaces.* The Journal of Adhesion, 2010. **86**(1): p. 39-61.
18. Spearing, S.M., *Materials Issues in MEMS.* Acta Materialia, 2000. **48**: p. 179-196.
19. Maboudian, R., *Surface Processes in MEMS Technology.* Surface Sci. Reports, 1998. **30**: p. 207.
20. R. Maboudian, W.R.A.a.C.C., *Self assembled monolayers as anti stiction coating for MEMS,characteristics and recent developments.* Sensors Actuators, 2009. **A82**: p. 219.
21. Howe, R.M.a.R.T., *Critical review: Adhesion in surface micromechanical structures.* J. Vac. Sci. Technol, 1997. **15**: p. 1.
22. YP, Z., *Morphological stability of epitaxial thin elastic films by van der Waals force.* Arch Appl Mech, 2002. **72**: p. 77.
23. Zhao, Y.-P.W., L. S. Yu, T. X., *Mechanics of adhesion in MEMS a review.* Journal of Adhesion Science and Technology, 2003. **17**(4): p. 519-546.

24. Christian Greiner, A.D.C., and Eduard Arzt, *Adhesion of bioinspired micropatterned surfaces: effects of pillar radius, aspect ratio, and preload.* Langmuir : the ACS journal of surfaces and colloids, 2007. **23(7)**: p. 3495–502.

25. J E Shigley, C.R.M., R G Budynas, X Liu, and Z Gao., *Mechanical engineering design* McGraw-Hill New York, 1989. **779**.

26. N J Glassmaker, T.H., C-Y Hui, and J Kim., *Design of biomimetic fibrillar interfaces: 1. Making contact.* Journal of the Royal Society, Interface / the Royal Society, 2004. **1(1)**: p. 23–33.

27. G. Formicone, M.S., D. Vasileska, and D. Ferry., *Study of a 50 nm nMOSFET by ensemble Monte Carlo simulation including a new approach to surface roughness and impurity scattering in the Si inversion layer.* IEEE Transactions on Electron Devices, 2002.

28. Dornfeld, D., *Material removal mechanism in chemical mechanical polishing: theory and modeling.* IEEE Transactions on Semiconductor Manufacturing,, 2001.

29. A. Asenov and S. Kaya. Asenov , A.a.K., K . *Effect of oxide interface roughness on the threshold voltage fluctuations in decanano MOSFETs with ultrathin gate oxides.* In , International Conference on Simulation of Semiconductor Effect of Oxide Interface Roughne, 2000: p. 135–138.

30. Amaral, R., *Surface Roughness.* 2002.

31. Grebe., P.C.P.a.a., *Application of time delay spectrometry for rough surface characterization.* Ultrasonics, 2001.

32. D. Bergström, J.P., and A. F.H. Kaplan, *The absorption of light by rough metal surfaces—A three-dimensional raytracing analysis.* J. Appl. Phys., 2008. **103**.

33. Y. P. Zhao, L.S.W., and T. X. Yu., *Mechanics of adhesion in MEMS—a review.* Journal of Adhesion Science and Technology, 2003.

34. Garcia N, S.E., *Monte Carlo Calculation for Electromagnetic-Wave Scattering from Random Rough Surfaces.* Phys. Rev. Lett, 1984. **52(20)**: p. 1798–801.

35. Bergstrom D, P.J., Kaplan AF., *The absorption of light by rough metal surfaces: A three-dimensional ray-tracing analysis.* J. App. Phys. 2008, 2008. **103(10)**.

36. Johnson., M.F.a.S., *The Design and Implementation of FFTW3.* Proceedings of the IEEE Transactions on Electron Devices, 2005.

37. Johnson, K.L., *Contact Mechanics.* 1985: Cambridge University Press.

38. Popov, V.L., *Contact Mechanics and Friction. Physical Principles and Applications.* Springer-Verlag, 2010.

39. Hertz, H., *Über die berührung fester elastischer Körper (On the contact of rigid elastic solids). .* 1896, London: Macmillan.

40. Maugis, D., *Contact, Adhesion and Rupture of Elastic Solids.* 2000, Berlin: Springer-Verlag, Solid-State Sciences.

41. Tang, T., Hui, C.-Y. & Glassmaker N.J., *Can a fibrillar interface be stronger and tougher than a non-fibrillar one?* J. Roy. Soc., 2005. **2**: p. 505-516.

42. Aksak, B., Chung, Y.H., Sitti, M., *The effect of aspect ratio on adhesion and stiffness for soft elastic fibres ?* J. Roy. Soc., 2011. **61**: p. 1166-1175.

43. Bogy, D.B.W., K. C., *Stress singularities at interface corners in bonded dissimilar isotropic elastic materials.* Int. J. Solids Struct. **7**: p. 993-1005.

44. Sümer, B., Aksak, B., Şahin, K., Chuengsatiansup, K., and Sitti, M., *Piezoelectric Polymer Fiber Arrays for Tactile Sensing Applications.* Sens. Lett, 2011. **9**: p. 547-463.

Resume

Credentials

Name Surname: Peyman Ansari

Place of birth: Tabriz

Marital status: Single

Email: p.ansari@hacettepe.edu.tr

Address: Mechanical engineering department – no. A430 – Hacettepe university – Beytepe – Ankara - Turkey

Education

High school: Sigatolislam

Undergraduate: Tabriz azad university

Master of Science: Hacettepe university

Foreign language and its level: English (very good) – Arabic (primary) – Farsi (perfect)

Work experience: Research assistant in mechanical engineering department of Hacettepe university (non staff) – President of Oljay Azer Ish engineering company.

Areas of expertise: Design, fabrication and characterization in micro-nano engineering.

Produced projects from thesis and their budgets: -

Publications from thesis: Ansari, P., Sümer, B., *Elastic Contact of Fibrillar Features on Rough Surface.*, World Tribology Congress 2013 Torino, Italy

Attended meetings with poster presentation and/or produced notifications from thesis: Sümer, B., <u>Ansari, P.</u>, Türkyılmaz, S., Korkmaz, Z., M.Koç, İ., *Design and Fabrication of Bio-Inspired Micro-Nano Polymer Fiber Array with Integrated Tactile Sensing Capability.*, 8th Nanoscience and Nanotechnology Congress 2012 Ankara, Turkey